Numerical Evaluation of Nonlinear Corrections to the DGLAP Equations for Nuclear PDFs

Bachelor's Thesis

Author: Janik Rausch
Supervisor: Dr. Vadim Guzey
First Examiner: Prof. Dr. André Eckardt
Second Examiner: Prof. Dr. Michael Klasen

Declaration of Academic Integrity

I hereby confirm that I wrote this thesis on my own, without any unlicensed help and using only the sources and aids stated.

Berlin, 11.03.2022

(signature of student)

Contents

1 Introduction

As of our current understanding, the atomic nucleus consists of protons and neutrons. These nucleons are in turn made up of quarks and gluons (collectively referred to as partons), held together by the strong interaction. A central goal of modern nuclear physics is understanding the partons within the nucleus in terms of Quantum Chromodynamics (QCD), a renormisable non-abelian gauge theory [1, 2].

The cleanest way to study QCD experimentally is deep inelastic scattering (DIS), where a beam of high-energy leptons is scattered off hadrons (i.e. particles composed of quarks). The reaction proceeds via an exchange of a virtual photon with the virtuality Q^2, which dissociates the hadron target. The DIS cross section depends on the structure functions F_1 and F_2, which are related to the partonic components of the hadron.

Before the advent of QCD, the parton model was proposed to explain the experimentally observed approximate Bjorken scaling (independence of Q^2) of the structure functions. Within this model, F_1 and F_2 can be expressed in terms of process-independent parton distribution functions (PDFs) corresponding to the probability that a parton carries a fraction x of the total hadron momentum [1]. These PDFs depend only on x as a consequence of the assumed limited values of parton transverse momenta.

The QCD factorisation theorem implies such PDFs can also be introduced in QCD [3]. The probabilistic interpretation of the parton model is strictly applicable only at leading order though, and the parton emission processes of QCD give rise to a dependence on the resolution scale Q^2. The associated coefficient functions can be obtained using perturbation theory (due to the asymptotic freedom of QCD), but the PDFs themselves cannot be calculated from first principles (except in lattice QCD). Nevertheless, it is possible to derive equations describing how the PDFs evolve when Q^2 changes.

To achieve this, the QCD emission processes are usually evaluated using the leading logarithmic approximation, where only "ladder" Feynman diagrams contribute. Assuming the momenta of the emitted partons are strongly ordered and summing up the corresponding collinear divergences leads to the Dokshitzer-Gribov-Lipatov-Altarelli-Parisi (DGLAP) equations which govern the Q^2 evolution of the PDFs [4, 5, 6]. They have been studied extensively and applied to various global PDF fits since their derivation.

The DGLAP equations are not the complete picture though, especially at very high energies or at very small x. For instance, one QCD process that the DGLAP equations don't account for is gluon recombination. At small x, the gluon density becomes high and there is a large probability for two gluons to fuse together, leading to a reduction of the gluon density. This can be addressed by analysing "fan" diagrams where two gluon ladders merge into a gluon or a quark-antiquark pair, resulting in the Gribov-Ryskin-Levin-Mueller-Qiu (GLR-MQ) equations [7, 8]. They act as a correction to the DGLAP equations and contain extra terms that are quadratic in the gluon distribution.

In this thesis, the DGLAP and the GLR-MQ equations are solved numerically at next-to-leading order (NLO) with python 3.8, using the same "brute force" method as the program QCDNUM16 [9]. The main focus is the impact of different parameters (i.e. the evolution direction, the presence of parton mixing and the nuclear mass number A) on the evolution. Furthermore, F_2 and $F_L \equiv F_2 - 2xF_1$ are calculated with the resulting PDFs and compared to accelerator data from HERA, and predictions concerning the scattering of heavy nuclei at the future facilities EIC and LHeC are made.

2 Background

The basic terms and concepts needed to understand parton evolution are introduced in this section. It is based on refs. [1], [2], [10] and [11].

2.1 Quantum Field Theory

Quantum field theory (QFT) is the modern framework of relativistic quantum mechanics. In QFT, particles are described by fields $\phi_i(x)$, the dynamics of which are dictated by the Euler-Lagrange equations of classical field theory. They are given by

$$\frac{\partial \mathscr{L}}{\partial \phi_i} - \frac{\mathrm{d}}{\mathrm{d}x^\mu} \frac{\partial \mathscr{L}}{\partial(\partial_\mu \phi_i)} = 0, \tag{2.1}$$

where $\mathscr{L}(\phi, \partial_\nu \phi)$ is the Lagrangian, a central object of any QFT.

The transition to a quantum theory can be achieved via the canonical quantisation, where the fields (and their conjugated momenta) are replaced by operators satisfying a canonical commutation relation. Generally such theories cannot be solved exactly, which means perturbation theory must be applied in order to derive predictions.

Free spin 1/2 particles are described by the Dirac Lagrangian

$$\mathscr{L}_0 = \overline{\Psi}(x)\big(i\partial\!\!\!/ - m\big)\Psi(x), \tag{2.2}$$

where $\Psi, \overline{\Psi}$ are four-component spinors and the "Feynman-slash" notation is defined as $a\!\!\!/ = \gamma^\mu a_\mu$ for any four-vector. Here and in the following, natural units with $c = \hbar = 1$ are used. Inserting $\mathscr{L}_0$ into the Euler-Lagrange field equations yields the Dirac equation. To derive interaction terms for these particles, certain symmetry ("gauge") transformations can be used, leading to the theories of Quantum Electrodynamics (QED) and Quantum Chromodynamics (QCD).

To obtain the Lagrangian for QED, one demands $\mathscr{L}_0$ to be invariant under local U(1) phase transformations. This is achieved by combining it with the Lagrangian of classical electrodynamics and including an interaction term, giving

$$\mathscr{L}_{\mathrm{QED}} = \overline{\Psi}(x)\big(iD\!\!\!/ - m\big)\Psi(x) - \frac{1}{4} F_{\mu\nu} F^{\mu\nu}. \tag{2.3}$$

Here, $D_\mu = \partial_\mu + igA_\mu$ is the covariant derivative and $F_{\mu\nu} = \partial_\mu A_\nu - \partial_\nu A_\mu$ is the electromagnetic field strength tensor. The QED Lagrangian describes electrically charged fermions interacting through electromagnetic spin 1 fields (photons in the quantised theory).

A similar procedure gives rise to QCD, this time using the group SU(3) instead of U(1). The resulting Lagrangian (for one quark flavor) is

$$\mathscr{L}_{\mathrm{QCD}} = \overline{\Psi}(x)(iD\!\!\!/ - m)\Psi(x) - \frac{1}{4} G^a_{\mu\nu} G^{\mu\nu}_a, \tag{2.4}$$

with the covariant derivative $D_\mu = \partial_\mu - ig_s A^a_\mu T^a$ (where A^a_μ are the gluon fields and T^a the generators of SU(3)) and the gluon field strength tensor $G^a_{\mu\nu} = \partial_\mu A^a_\nu - \partial_\nu A^a_\mu + g_s f_{abc} A^b_\mu A^c_\nu$. It corresponds to colored quarks and gluons and the strong interaction between them.

Despite the similar structure of these Lagrangians, there are great qualitative differences between the two theories. The non-Abelian nature of SU(3) introduces gluon self-interaction, which has no QED analogue. This leads to a logarithmic decrease of the QCD coupling parameter when the momentum transfer Q^2 increases: At NLO, $\alpha_s \equiv g_s^2/4\pi$ is given by [3]

$$\frac{\alpha_s(Q^2)}{4\pi} = \frac{1}{\beta_1 \ln(Q^2/\Lambda^2)} - \frac{\beta_2 \ln\left(\ln(Q^2/\Lambda^2)\right)}{\beta_1^3 \ln^2(Q^2/\Lambda^2)}, \tag{2.5}$$

with the beta functions $\beta_1 = 11 - 2N_F/3$ and $\beta_2 = 102 - 38N_F/3$, where N_F is the number of active flavors (i.e. of quarks with $m < Q$). The QCD scale parameter Λ also depends on N_F. From here on the Q^2 dependence of α_s won't be written explicitly.

The behavior of α_s gives rise to the important phenomena of asymptotic freedom and confinement. The former means that the coupling is weak at high Q^2, which enables the use of perturbation theory in this region; the latter expresses the fact that free quarks don't occur in nature because the coupling becomes stronger when the separation $r^2 \propto 1/Q^2$ between quarks increases.

The predictions of QCD and other quantum field theories are most commonly tested in scattering experiments, where particles are accelerated to very high speeds before colliding with each other. The corresponding theoretical quantity is the differential cross section, i.e. the rate at which a certain interaction between particles occurs. It can be written as

$$\mathrm{d}\sigma = \frac{1}{F}|\mathcal{M}|^2 \,\mathrm{dLips}\,, \tag{2.6}$$

where F is the flux of incoming particles, dLips the Lorentz invariant phase space element of the final state particles and $\mathcal{M}$ the invariant amplitude. The latter is closely related to the scattering matrix, which connects incoming and outgoing particle states.

The invariant amplitude can be obtained from a Feynman diagram, a pictorial representation of the scattering process in question. This is done using Feynman rules, which follow from the quantised Lagrangian and assign a factor to every line and vertex of the diagram.

2.2 Electron-Proton DIS

The inner structure of a proton can be probed by scattering a beam of high-energy electrons off it. If the momentum transfer is high enough, the proton breaks apart into its constituent particles, which is known as deep inelastic scattering (DIS). The Feynman diagram of this process is shown in fig. 1, where X denotes the unknown many-particle final state of the proton.

For the evaluation of the diagram, the invariant kinematic variables

$$Q^2 = -q^2, \quad x = \frac{Q^2}{2(p \cdot q)}, \quad y = \frac{p \cdot q}{p \cdot k} \tag{2.7}$$

are used, which can be interpreted as follows: Q^2 is the photon virtuality and serves as the hard resolution scale for the collision; x is the Bjorken variable, which (within the parton model, see sec. 2.3) is equal to the longitudinal fraction of p carried by the interacting

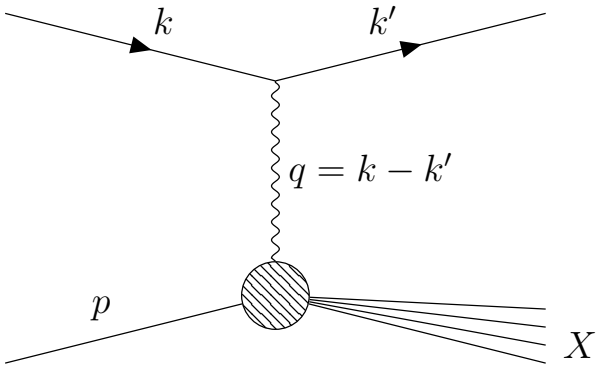

Fig. 1: Feynman diagram of electron-proton deep inelastic scattering, where X stands for all possible proton final states.

parton; y is the longitudinal fraction of k carried by the photon. In the proton rest frame, the involved four-momenta can be written as

$$p = (M, 0, 0, 0), \tag{2.8}$$
$$k = (E, 0, 0, E), \tag{2.9}$$
$$k' = (E', E' \sin\theta \cos\varphi, E' \sin\theta \sin\varphi, E' \cos\theta), \tag{2.10}$$

where M is the invariant mass of the proton. The electron mass m is neglected since it is very small compared to M and Q. The kinematic variables in this frame are

$$Q^2 = 2EE'(1 - \cos\theta), \quad x = \frac{Q^2}{2M\nu}, \quad y = \frac{\nu}{E}, \tag{2.11}$$

with $\nu = E - E'$.

To calculate the cross section for this process with eq. (2.6), $F = 4(k \cdot p)$ and

$$\mathrm{dLips} = \Pi^3 k' \sum_N \int \prod_{n=1}^{N} \left(\Pi^3 p_n\right) (2\pi)^4 \delta^{(4)} \left(p + q - \sum_{n=1}^{N} p_n\right) \tag{2.12}$$
$$= \Pi^3 k' \sum_X \Pi^3 p_X (2\pi)^4 \delta^{(4)}(p + q - p_X), \tag{2.13}$$

are used, where the "sum" in dLips takes all possible N-particle proton final states into account. The Lorentz invariant integral measure $\Pi^3 k_i$ is given by

$$\Pi^3 k_i = \frac{\mathrm{d}^3 k_i}{(2\pi)^3 2E(k_i)} \tag{2.14}$$

for any four-momentum k_i. The QED Feynman rules yield

$$\mathcal{M} = \frac{e^2}{q^2} \overline{u}(k') \gamma^\mu u(k) \left\langle X | J_\mu | p \right\rangle, \tag{2.15}$$

where the expression for the proton vertex is kept very general since no assumptions have been made about its inner structure. In the following, unpolarised scattering is

considered, i.e. $|\mathcal{M}|^2$ is averaged over initial state polarisations and summed over final state polarisations (denoted by s_i and s_f).

Inserting F, dLips and $\mathcal{M}$ into eq. (2.6) gives

$$\mathrm{d}\sigma = \frac{1}{4(k\cdot p)}\frac{e^4}{q^4} 4\pi M L^{\mu\nu} W_{\mu\nu}\, \Pi^3 k', \tag{2.16}$$

where $L^{\mu\nu}, W_{\mu\nu}$ are the leptonic and hadronic tensor. They contain the terms associated with the electron and proton vertex in the diagram respectively, i.e.

$$L^{\mu\nu} = \frac{1}{2}\sum_{s_i,s_f} \overline{u}(k)\gamma^\nu u(k')\overline{u}(k')\gamma^\mu u(k), \tag{2.17}$$

$$W_{\mu\nu} = \frac{1}{4\pi M}\sum_X \Pi^3 p_X (2\pi)^4 \delta^{(4)}(p+q-p_X)\frac{1}{2}\sum_{s_i,s_f}\langle p|J_\mu^\dagger|X\rangle\langle X|J_\nu|p\rangle\,. \tag{2.18}$$

The spin sums in $L^{\mu\nu}$ can be written as a trace using the completeness relations for Dirac spinors, and $W_{\mu\nu}$ can be expressed in terms of independent Lorentz structures and simplified by demanding current conservation at the proton vertex. This results in

$$L^{\mu\nu} = \frac{1}{2}\,\mathrm{tr}(\not{k}'\gamma^\mu \not{k}\gamma^\nu) = 2\big(k'^\mu k^\nu + k'^\nu k^\mu - (k'\cdot k)g^{\mu\nu}\big), \tag{2.19}$$

$$W_{\mu\nu} = \frac{F_1}{M}\left(-g_{\mu\nu}+\frac{q_\mu q_\nu}{q^2}\right) + \frac{F_2}{\nu M^2}\left(p_\mu - \frac{p\cdot q}{q^2}q_\mu\right)\left(p_\nu - \frac{p\cdot q}{q^2}q_\nu\right), \tag{2.20}$$

where F_1 and F_2 are parameters known as structure functions, which express the lack of knowledge about the constituent particles of the proton. The tensors $L^{\mu\nu}$ and $W_{\mu\nu}$ can now be contracted. Furthermore, using the transformation $(x, Q^2) \to (E', \cos\theta)$ given by eq. (2.11), the phase space factor $\Pi^3 k'$ is rewritten in terms of the variables x and Q^2. Evaluating the corresponding Jacobian gives

$$\mathrm{d}^3 k' = E'^2\,\mathrm{d}E'\,\mathrm{d}\cos\theta\,\mathrm{d}\varphi = 2\pi\frac{M}{Q^2}EE'y^2\,\mathrm{d}x\,\mathrm{d}Q^2\,, \tag{2.21}$$

where $\mathrm{d}\varphi = 2\pi$ since the results of unpolarised scattering are independent of the angle φ.

Taking all this into account, the cross section in eq. (2.16) becomes

$$\frac{\mathrm{d}\sigma}{\mathrm{d}x\mathrm{d}Q^2} = \frac{e^4}{2\pi x Q^4}\left[xy^2F_1 + \left(1-y-\frac{x^2y^2M^2}{Q^2}\right)F_2\right]. \tag{2.22}$$

To derive predictions for scattering experiments from this equation, F_1 and F_2 must be computed, so a model for the inner structure of the proton is needed.

2.3 Parton Model

The parton model predates QCD, and its basic assumption is that the proton consists of non-interacting partons. This can be justified by using the infinite momentum frame, where the interaction time between partons is large compared to that of the incoming photon. The partons were later identified with the quarks observed in hadron spectroscopy experiments; within QCD, the term parton refers to both quarks and gluons.

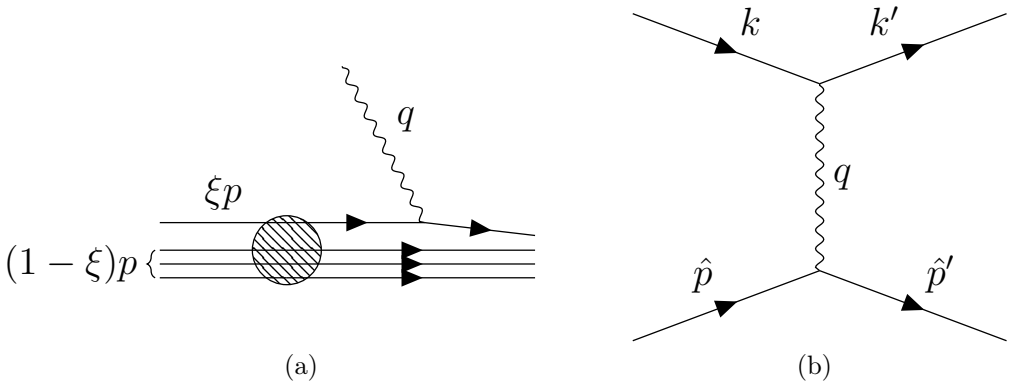

Fig. 2: (a) Interpretation of the PDFs, (b) elastic electron-quark scattering.

The parton model allows the electron-proton DIS cross section to be expressed in terms of parton distribution functions (PDFs) $q_i(\xi)$, which correspond to the probability that quark i has momentum $\hat{p} = \xi p$, see fig. 2a. The transverse component of the parton momentum is neglected, which implies the PDFs don't depend on Q^2 in the parton model. An important constraint on the PDFs is given by the sum rule

$$\sum_i \int_0^1 \mathrm{d}\xi \, \xi q_i(\xi, Q^2) = 1, \tag{2.23}$$

which follows from momentum conservation.

With the PDFs, the DIS cross section can be written as

$$\frac{\mathrm{d}\sigma}{\mathrm{d}x\mathrm{d}Q^2} = \sum_i \int_0^1 \mathrm{d}\xi \, q_i(\xi) \frac{\mathrm{d}\hat{\sigma}_i}{\mathrm{d}x\mathrm{d}Q^2}, \tag{2.24}$$

where the last term is the cross section for elastic electron-quark scattering, which can be derived from the diagram in fig. 2b using the Feynman rules of QED. The necessary elements are

$$F = 4(k \cdot \hat{p}), \tag{2.25}$$

$$\mathcal{M} = \frac{e^2 e_i}{q^2} \, \overline{u}(k')\gamma^\mu u(k) \overline{u}(\hat{p}')\gamma_\mu u(\hat{p}), \tag{2.26}$$

$$\mathrm{dLips} = \Pi^3 k' \, \Pi^3 \hat{p}' \, (2\pi)^4 \delta^{(4)}(\hat{p} + q - \hat{p}'). \tag{2.27}$$

Inserting them into eq. (2.6), using

$$\frac{\mathrm{d}^3\hat{p}'}{2E(\hat{p}')} = \delta(\hat{p}'^2) \, \Theta\big(E(\hat{p}')\big) \, \mathrm{d}^4\hat{p}' \tag{2.28}$$

and $(\hat{p} + q)^2 \approx Q^2/x(\xi - x)$ to evaluate the delta function in dLips and again neglecting the electron mass gives

$$\frac{\mathrm{d}\hat{\sigma}_i}{\mathrm{d}x\mathrm{d}Q^2} = \frac{e^4 e_i^2}{4\pi Q^4} \left[1 - y + y^2 \left(\frac{1}{2} - \frac{x^2 M^2}{Q^2}\right)\right] \delta(\xi - x). \tag{2.29}$$

The remaining delta function implies that ξ is equal to the variable x from the previous section, fixed by external kinematics.

With this, one obtains

$$\frac{\mathrm{d}\sigma}{\mathrm{d}x\mathrm{d}Q^2} = \frac{e^4}{4\pi Q^4}\left[1 - y + y^2\left(\frac{1}{2} - \frac{x^2M^2}{Q^2}\right)\right]\sum_i e_i^2 q_i(x) \tag{2.30}$$

$$\equiv \frac{\mathrm{d}\hat{\sigma}_0}{\mathrm{d}x\mathrm{d}Q^2}\sum_i e_i^2 q_i(x) \tag{2.31}$$

from eq. (2.24). Comparing eqs. (2.30) and (2.22) yields the Callan-Gross relation

$$2xF_1(x) = F_2(x) = x\sum_i e_i^2 q_i(x), \tag{2.32}$$

which shows that the structure functions only depend on x in the parton model, a property known as Bjorken scaling. Eq. (2.32) follows from the assumption that partons have spin $1/2$ and agrees well with experimental data, confirming the identification of partons with quarks. Bjorken scaling is violated when QCD interactions between quarks are taken into account.

The calculations of this section can be generalised to the case of heavier nuclei with mass number $A > 1$. However, the corresponding PDFs aren't simple superpositions of free proton and neutron PDFs [12]. This observation is known to be caused by effects such as nuclear shadowing/antishadowing, EMC suppression and Fermi motion [13, 14].

3 Evolution Equations in QCD

In this section, QCD corrections to the parton model are discussed. Most importantly, the derivation of the DGLAP and the GLR-MQ equations is sketched.

3.1 DGLAP Equations

Partons interact via the QCD processes pictured in fig. 3, leading to a Q^2 dependence of the PDFs. This effect is usually evaluated in the leading logarithmic approximation (LLA). In this framework, only terms proportional to $(\alpha_s \log Q^2)^n$ are considered, neglecting those where α_s isn't compensated by a large logarithm [15]. This corresponds to resumming the divergences caused by collinear parton emission.

To evaluate processes like this, the axial gauge is commonly used since it only involves physical gluon polarisations, so there is no need to introduce ghost particles [3]. In this gauge, "ladder" type diagrams are the only ones contributing to the LLA [11, 15], and the gluon propagator is given by

$$D_{\mu\nu}(k) = \frac{-i\delta_{ab}}{k^2 + i\epsilon} P_{\mu\nu}(k), \tag{3.1}$$

$$P_{\mu\nu}(k) = g_{\mu\nu} - \frac{k_\mu \eta_\nu - k_\nu \eta_\mu}{\eta \cdot k}, \tag{3.2}$$

where η is a light-cone four-vector. The cut diagram notation, where both $\mathcal{M}$ and $\mathcal{M}^*$ are combined in a single diagram [3], is used to simplify the calculations.

Fig. 4 contains three gluon emission diagrams. Only fig. 4a is a ladder diagram, so only it must be evaluated. The invariant amplitude matrix element follows from the Feynman rules for QCD and can be written as [11]

$$|\mathcal{M}|^2_{\mu\nu} = g_s^2 \frac{2(1-z)}{-k_\perp^2} P_{FF}(x) \frac{e_i^2}{2} \operatorname{tr}(\not{p}' \gamma_\mu \not{p} \gamma_\nu), \tag{3.3}$$

where $P_{FF}(x) = C_F(1+x^2)/(1-x)$ is the leading order quark-quark splitting function (with the color factor $C_F = 4/3$). The singularity at $x = 1$ is canceled by virtual gluon emission diagrams [1, 11], giving a slightly different expression which can be found in the appendix (sec. 7.1).

Calculating the corresponding modification to the DIS cross section and adding it to the parton model result from eq. (2.30) yields [11]

$$\frac{\mathrm{d}\sigma}{\mathrm{d}x\mathrm{d}Q^2} = \frac{\mathrm{d}\hat{\sigma}_0}{\mathrm{d}x\mathrm{d}Q^2} \sum_i e_i^2 \left[\delta(1-x) + \frac{\alpha_s}{2\pi} \ln\left(\frac{Q^2}{m^2}\right) P_{FF}(x) \right] \otimes q_i(x), \tag{3.4}$$

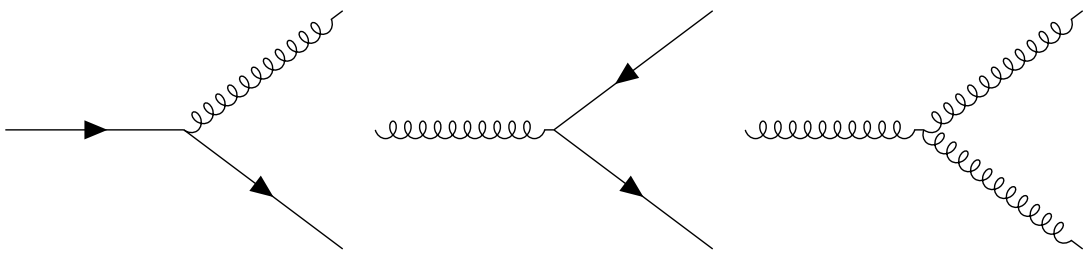

Fig. 3: QCD vertices that influence DGLAP parton evolution [10].

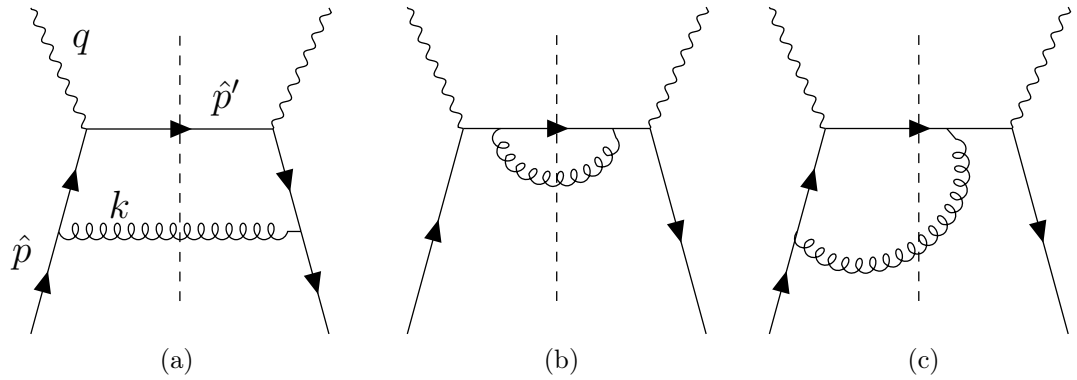

Fig. 4: Gluon emission diagrams (in the cut diagram notation): (a) ladder diagram contributing to the LLA, (b)&(c) non-ladder diagrams [11].

where the convolution $\otimes$ is defined as

$$f(x) \otimes g(x) = \int_x^1 \frac{\mathrm{d}z}{z} f(z)\, g\Big(\frac{x}{z}\Big) = g(x) \otimes f(x). \tag{3.5}$$

The logarithmic term originates from the integral

$$\int_{m^2}^{Q^2} \frac{\mathrm{d}\mathbf{k}_\perp^2}{\mathbf{k}_\perp^2} = \ln\left(\frac{Q^2}{m^2}\right), \tag{3.6}$$

which is related to the collinear divergence of the quark propagator due to gluon radiation. Eq. (3.4) suggests $(\alpha_s/2\pi)\ln(Q^2/m^2)P_{FF}(x)$ can be understood as the probability density that the quark emits a gluon with momentum $(1-x)\hat{p}$ [1, 11].

It is also possible for the quark to emit multiple gluons before interacting with the photon, as shown in fig. 5a. To obtain a LLA contribution from this Feynman diagram, the transverse momenta of the n emitted gluons must be strongly ordered,

$$-k_{\perp 1}^2 \ll -k_{\perp 2}^2 \ll \ldots \ll -k_{\perp n}^2 \ll Q^2. \tag{3.7}$$

The momentum fractions x_i decrease similarly with each emission. When taking all such ladder diagrams into account, one obtains an exponential series [11], i.e.

$$\frac{\mathrm{d}\sigma}{\mathrm{d}x\mathrm{d}Q^2} = \frac{\mathrm{d}\hat{\sigma}_0}{\mathrm{d}x\mathrm{d}Q^2} \sum_i e_i^2 \exp\left[\frac{\alpha_s}{2\pi} \ln\left(\frac{Q^2}{m^2}\right) P_{FF}(x)\right] \otimes q_i(x). \tag{3.8}$$

This corresponds to making the replacement

$$q_i(x) \to q_i(x, Q^2) = \exp\left[\frac{\alpha_s}{2\pi} \ln\left(\frac{Q^2}{m^2}\right) P_{FF}(x)\right] \otimes q_i(x) \tag{3.9}$$

in eq. (2.30), which implies the DGLAP equation of q-q splitting [11]:

$$\frac{\partial}{\partial \ln Q^2}\, q_i(x, Q^2) = \frac{\alpha_s}{2\pi} P_{FF}(x) \otimes q_i(x, Q^2). \tag{3.10}$$

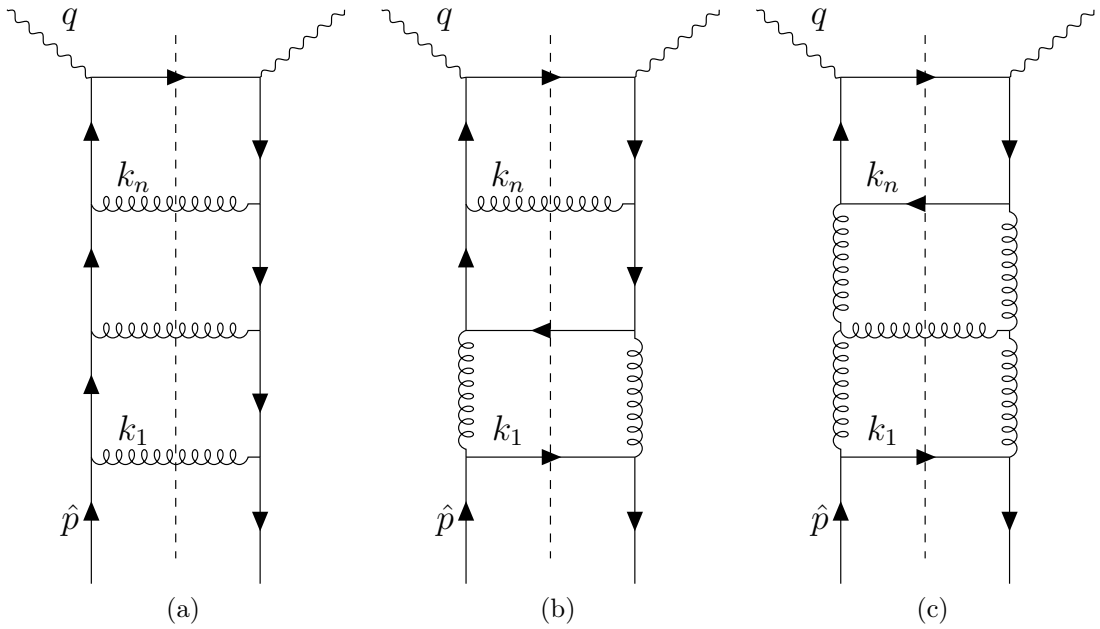

Fig. 5: Ladder diagrams illustrating different contributions to the LLA (in the cut diagram notation): (a) three q-q splitting cells, (b) q-g, g-q and q-q cells, (c) q-g, g-g and g-q cells [15, 11].

The Feynman diagrams for g-q, q-g and g-g splitting can be evaluated similarly, introducing the respective splitting functions P_{FG}, P_{GF} and P_{GG} (see sec. 7.1) and the gluon PDF $g(x, Q^2)$. Combinations of different emission processes are also possible, as illustrated in figs. 5b and 5c. This can be adressed by defining $q_i(x, Q^2)$ and $g(x, Q^2)$ as the exponential of a matrix containing all splitting functions, a generalisation of eq. (3.9) resulting in the full DGLAP evolution equations [11],

$$\frac{\partial}{\partial \ln Q^2} q_i(x, Q^2) = \frac{\alpha_s}{2\pi}\left[\sum_j P_{FF}(x) \otimes q_j(x) + P_{FG}(x) \otimes g(x, Q^2)\right] \tag{3.11}$$

$$\frac{\partial}{\partial \ln Q^2} g(x, Q^2) = \frac{\alpha_s}{2\pi}\left[\sum_j P_{GF}(x) \otimes q_j(x) + P_{GG}(x) \otimes g(x, Q^2)\right]. \tag{3.12}$$

As mentioned before, the functions P_{AB} are related to the probabilities of the different parton emission processes. This shows how the DGLAP equations can be interpreted in terms of fig. 3: The convolution integrals on the r.h.s. give the total amount of partons with momentum fraction x emitted by other partons with fractions $z > x$.

The equations can be written in a compact form by introducing the singlet quark distribution

$$\Sigma(x, Q^2) = \sum_{i=1}^{N_F} \left(q_i(x, Q^2) + \overline{q}_i(x, Q^2)\right) \tag{3.13}$$

as well as the nonsinglet distributions

$$q_i^-(x, Q^2) = q_i(x, Q^2) - \overline{q}_i(x, Q^2) \tag{3.14}$$

$$q_i^+(x, Q^2) = q_i(x, Q^2) + \overline{q}_i(x, Q^2) - \frac{1}{N_F}\Sigma(x, Q^2), \tag{3.15}$$

where $\overline{q}_i$ denotes the antiquark PDFs. The DGLAP equations in terms of these linear combinations are given by [16]

$$\frac{\partial}{\partial \ln Q^2}\begin{pmatrix}\Sigma(x,Q^2)\\ g(x,Q^2)\end{pmatrix} = \frac{\alpha_s}{2\pi}\begin{pmatrix}P_{FF}(x) & P_{FG}(x)\\ P_{GF}(x) & P_{GG}(x)\end{pmatrix} \otimes \begin{pmatrix}\Sigma(x,Q^2)\\ g(x,Q^2)\end{pmatrix}, \tag{3.16}$$

$$\frac{\partial}{\partial \ln Q^2}\, q_i^{\pm}(x,Q^2) = \frac{\alpha_s}{2\pi} P_{\pm}(x) \otimes q_i^{\pm}(x,Q^2). \tag{3.17}$$

It is important to note that PDFs are non-perturbative, so some external input is always required to compute solutions of the DGLAP equations. In this thesis, PDFs from the nCTEQ15 collaboration (generated with the LHAPDF6 library [17]) are used as initial conditions for the evolution, which were obtained by using the DGLAP equations as well as various experimental data [13].

Evolving the initial values upward (towards higher Q^2) with the DGLAP equations corresponds to increasing the "resolution" of the scattering experiment. The interactions between partons affect the PDFs more the higher Q^2 is [1]. Conversely, evolving downward from high Q^2 corresponds to a decrease in resolution. The non-interacting picture of the nucleus must be reproduced at low Q^2, so the downward evolution can be interpreted as the parton interactions happening in reverse.

Eq. (3.17) (the nonsinglet evolution equation) is independent of the gluon distribution. Since it also doesn't receive corrections due to gluon recombination [8], the nonsinglet PDFs can mostly be ignored in the context of this thesis. For convenience, the remaining DGLAP equations will be used in terms of the momentum densities $\Omega(x,Q^2) = x\Sigma(x,Q^2)$ and $G(x,Q^2) = xg(x,Q^2)$ from here on, i.e. [9]

$$\frac{\partial \Omega}{\partial \ln Q^2}(x,Q^2) = \frac{\alpha_s}{2\pi}\int_x^1 \frac{\mathrm{d}z}{z^2} x\left[P_{FF}\left(\frac{x}{z}\right)\Omega(z,Q^2) + P_{FG}\left(\frac{x}{z}\right)G(z,Q^2)\right] \tag{3.18}$$

$$\frac{\partial G}{\partial \ln Q^2}(x,Q^2) = \frac{\alpha_s}{2\pi}\int_x^1 \frac{\mathrm{d}z}{z^2} x\left[P_{GF}\left(\frac{x}{z}\right)\Omega(z,Q^2) + P_{GG}\left(\frac{x}{z}\right)G(z,Q^2)\right]. \tag{3.19}$$

3.2 GLR-MQ Equations

Apart from the processes discussed in the previous section (where one parton turns into two partons), it is also possible for two gluons to recombine into a single gluon or into a quark-antiquark pair. This affects the PDFs, especially in the limit of high gluon densities, when the wavefunctions spatially overlap.

One approach to address this fact leads to the GLR-MQ equations, where the merging of two DGLAP gluon ladders into a bare gluon or fermion cut vertex ("fan diagrams") is considered [7, 8]. This corresponds to graphs as those shown in fig. 6. They can be analysed with the QCD Feynman rules, analogously to the DGLAP equations. In the following, the central steps taken in the paper by Mueller and Qiu [8] to evaluate g-g recombination effects are presented.

First, the LLA contribution of the diagram in fig. 6a is derived, again using the axial

gauge (see eq. (3.1)). The part of the diagram with momentum labels gives

$$\begin{aligned} V = & \frac{k_{1\mu}^{\perp} k_{2\nu}^{\perp} k_{2\rho}^{\perp} k_{1\sigma}^{\perp}}{\eta \cdot k_1 \eta \cdot k_2 \eta \cdot (k_2+\delta)\, \eta \cdot (k_1-\delta)} \frac{g^4}{(2\pi)^4} \frac{C_G^2}{N^2-1} \\ & \times \int \mathrm{d}^4 l \, \frac{-2\pi\delta\left[(k_1+k_2-l)^2\right]}{\left[l^2+i\varepsilon\right]\left[l^2-i\varepsilon\right]\left[(k_1-l)^2+i\varepsilon\right]\left[(k_1-l-\delta)^2-i\varepsilon\right]} \\ & \times \Gamma_{\alpha\gamma\mu} P_{\gamma\delta} \Gamma_{\delta\xi\nu} P_{\xi\zeta} \Gamma_{\zeta\epsilon\rho} P_{\epsilon\lambda} \Gamma_{\lambda\beta\sigma} \frac{-\eta_\alpha \eta_\beta l^2}{(\eta \cdot l)^2} x \delta\left(x - \frac{\eta \cdot l}{\eta \cdot p}\right), \end{aligned} \tag{3.20}$$

where Γ denotes a three-gluon vertex, and the approximation

$$-2k_\alpha P_{\alpha\beta}(l) \approx \frac{2\eta \cdot k}{\eta \cdot l} l_\beta^{\perp} \tag{3.21}$$

is used to obtain the first term. The final term corresponds to the gluon cut vertex. In addition, the diagrams related to fig. 6a through the exchanges $k_1 \leftrightarrow k_2$, $k_1 - \delta \leftrightarrow k_2 + \delta$, and both of those at once must be taken into account, resulting in

$$\begin{aligned} V = & \frac{\underline{k}_1^2 \underline{k}_2^2 \left[\eta \cdot (k_1+k_2)^2 + \eta \cdot k_1\, \eta \cdot (k_1-\delta) + \eta \cdot k_2\, \eta \cdot (k_2+\delta)\right]}{\eta \cdot (k_1+k_2)\left[\eta \cdot k_1\, \eta \cdot k_2\, \eta \cdot (k_1-\delta)\, \eta \cdot (k_2+\delta)\right]^2} \\ & \times \left\{2\left[\eta \cdot (k_1+k_2)^2 - \eta \cdot k_1\, \eta \cdot (k_2+\delta)\right]\right. \\ & \left. \times \left[\eta \cdot (k_1+k_2)^2 - \eta \cdot k_2\, \eta \cdot (k_1-\delta)\right] + \left[\eta \cdot \delta\, \eta \cdot (k_1+k_2)\right]^2\right\} \\ & \times \alpha_s^2 \frac{2C_G^2}{N^2-1} \frac{1}{\eta \cdot l} \int^{Q^2} \frac{\mathrm{d}\underline{l}^2}{\left[\underline{l}^2\right]^2}. \end{aligned} \tag{3.22}$$

This expression is then integrated over k_{1-}, k_{2-} and δ_- (using light-cone coordinates $(v_-, v_+, \underline{v})$ with $\eta \cdot v = v_-$), yielding

$$I = \alpha_s^2 64\pi^4 \frac{C_G^2}{N^2-1} \frac{\underline{k}_1^2 \underline{k}_2^2}{\eta \cdot l} \int^{Q^2} \frac{\mathrm{d}\underline{l}^2}{\left[\underline{l}^2\right]^2} \int_x \frac{\mathrm{d}u}{u}. \tag{3.23}$$

Other g-g recombination diagrams were examined by Mueller and Qiu, but the corresponding integrals are equal to zero. Eq. (3.23) is now multiplied with

$$1 = \int \mathrm{d}k_{1-} \frac{\eta \cdot p}{(\eta \cdot k_1)^2} u^2 \delta\left(u - \frac{\eta \cdot k_1}{\eta \cdot p}\right) \int \mathrm{d}k_{2-} \frac{\eta \cdot p}{(\eta \cdot k_2)^2} u^2 \delta\left(u - \frac{\eta \cdot k_2}{\eta \cdot p}\right), \tag{3.24}$$

where

$$u = \frac{\eta \cdot (k_1+k_2)}{2\eta \cdot p}. \tag{3.25}$$

By applying the logarithmic derivative $\partial / \partial \ln Q^2$ to the result, one obtains the new contribution to the gluon evolution equation:

$$\frac{\partial G}{\partial \ln Q^2}(x, Q^2) = -4\pi\alpha_s^2 \frac{C_G^2}{N^2-1} \frac{1}{Q^2} \int_x^1 \frac{\mathrm{d}z}{z} z^2 g^{(2)}(z, Q^2), \tag{3.26}$$

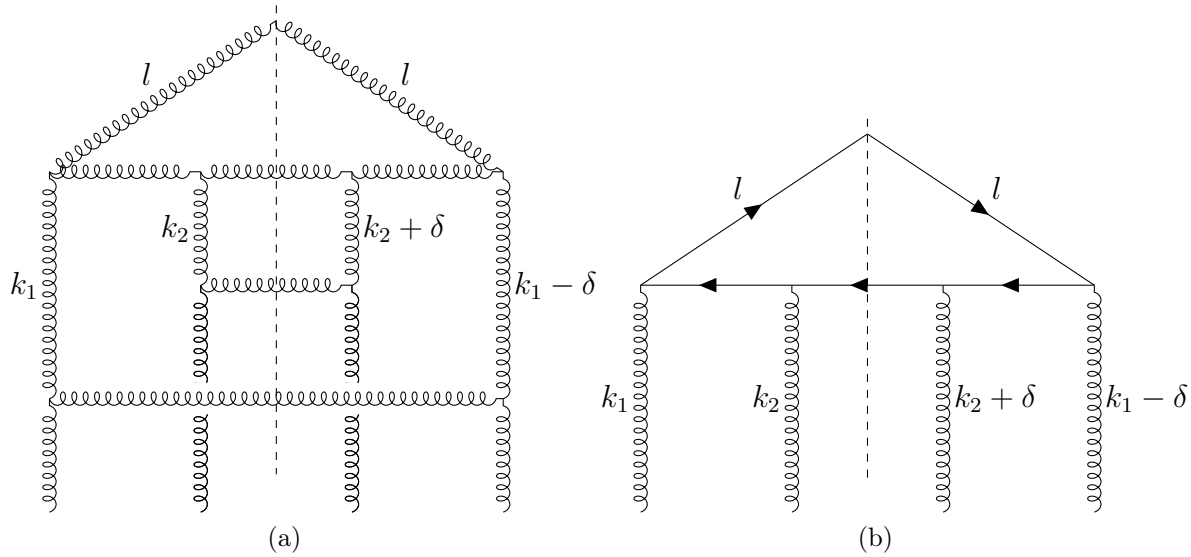

Fig. 6: Two diagrams used in the derivation of the GLR-MQ equations [8]: (a) g-g recombination, (b) g-q recombination.

where $g^{(2)}$ is the two-gluon distribution. In a low-density model of the nucleus, it is given by [18]

$$x^2 g^{(2)}(x, Q^2) = \frac{9}{8} \frac{1}{\pi R^2} \big(G(x, Q^2)\big)^2, \tag{3.27}$$

with the target radius R.

Similar calculations can be done for g-q recombination diagrams as illustrated in fig. 6b, leading to a correction to the quark singlet equation. The full GLR-MQ evolution equations can be written as [19]

$$\frac{\partial \Omega}{\partial \ln Q^2}(x, Q^2) = \frac{\partial \Omega}{\partial \ln Q^2}(x, Q^2)\bigg|_{\text{lin}} - \frac{27}{160} \frac{\alpha_s^2}{R^2 Q^2} \big(G(z, Q^2)\big)^2 \tag{3.28}$$

$$\frac{\partial G}{\partial \ln Q^2}(x, Q^2) = \frac{\partial G}{\partial \ln Q^2}(x, Q^2)\bigg|_{\text{lin}} - \frac{81}{16} \frac{\alpha_s^2}{R^2 Q^2} \int_x^1 \frac{\mathrm{d}z}{z} \big(G(z, Q^2)\big)^2, \tag{3.29}$$

where the first terms on the r.h.s. are given by the DGLAP equations. The positive g-q recombination term containing G_{HT} given by Mueller and Qiu is neglected here. Both of the new terms are nonlinear in the gluon distribution, so the resulting dynamics are expected to be quite different from the linear DGLAP equations.

The radius R can be approximated by $R = 1.25\,\text{fm} \cdot A^{1/3}$ (or $R = 6.34\,\text{GeV}^{-1} \cdot A^{1/3}$ in natural units), where A is the mass number of the nucleus. For convenience, the shorthand notation

$$f(Q^2) = \frac{\alpha_s^2}{R^2 Q^2} \tag{3.30}$$

is introduced. If the input PDFs are given in the form Ω/A and G/A (as is the case with the nCTEQ15 parametrisation), $f(Q^2)$ has to be multiplied by an additional factor A in the numerical evaluation.

There are other ways to analyse DIS in the high parton density limit. For example, the Balitsky-Kovchegov (BK) evolution equation can be obtained by treating the incoming photon as a quark-antiquark dipole. The structure of the BK equation is similar to GLR-MQ (the linear terms correspond to the BFKL equation and the nonlinear terms to parton ladder merging), and it has the same physical interpretation [20].

Another approach is to determine the change to the nuclear wave function ("color glass condensate") caused by an increase in energy. This leads to the Jalilian-Marian-Iancu-McLerran-Weigert-Leonidov-Kovner (JIMWLK) equation, which corresponds to the same processes as the BK equation [20].

3.3 NLO Structure Functions

As explained in section 2.3, the original purpose of PDFs is to enable the calculation of the nuclear structure functions F_1, F_2. This is still true in QCD, even though the parton model formula is replaced by a more general expression through the QCD factorisation theorem [3].

The NLO structure functions (in the $\overline{\text{MS}}$ factorisation scheme and assuming $Q_f^2 = Q^2$) can be written as [11]

$$2xF_1(x,Q^2) = F_2(x,Q^2) - x\sum_{i=1}^{N_F} e_i^2(q_i+\overline{q}_i) \otimes \left(\frac{\alpha_s}{2\pi}C_{Lq}^{(1)}\right) - x\left\langle e^2\right\rangle g \otimes \left(\frac{\alpha_s}{2\pi}C_{Lg}^{(1)}\right), \quad (3.31)$$

$$F_2(x,Q^2) = x\sum_{i=1}^{N_F} e_i^2(q_i+\overline{q}_i) \otimes \left(\delta(1-x) + \frac{\alpha_s}{2\pi}C_{2q}^{(1)}\right) + x\left\langle e^2\right\rangle g \otimes \left(\frac{\alpha_s}{2\pi}C_{2g}^{(1)}\right), \quad (3.32)$$

where the coefficient functions $C_{ij}^{(1)}$ are given in sec. 7.2 and

$$\left\langle e^2\right\rangle = \frac{1}{N_F}\sum_{i=1}^{N_F} e_i^2 \quad (3.33)$$

is the average of the squared quark charges. The leading order δ-term in F_2 corresponds to the Callan-Gross relation, see eq. (2.32). In most applications, the longitudinal structure function $F_L \equiv F_2 - 2xF_1$ is used instead of F_1.

To express F_2, F_L in terms of singlet and nonsinglet quark distributions, the $(q_i + \overline{q}_i)$ terms are rewritten with eq. (3.15). One obtains [9]

$$\begin{aligned} F_2(x,Q^2) = N(x,Q^2) &+ \frac{\alpha_s}{2\pi}\int_x^1 \frac{\mathrm{d}z}{z^2} xC_{2q}^{(1)}\left(\frac{x}{z}\right) N(z,Q^2) \\ &+ \left\langle e^2\right\rangle \Omega(x,Q^2) + \left\langle e^2\right\rangle \frac{\alpha_s}{2\pi}\int_x^1 \frac{\mathrm{d}z}{z^2} xC_{2q}^{(1)}\left(\frac{x}{z}\right)\Omega(z,Q^2) \\ &+ \left\langle e^2\right\rangle \frac{\alpha_s}{2\pi}\int_x^1 \frac{\mathrm{d}z}{z^2} xC_{2g}^{(1)}\left(\frac{x}{z}\right) G(z,Q^2) \end{aligned} \quad (3.34)$$

$$F_L(x,Q^2) = \frac{\alpha_s}{2\pi}\int_x^1 \frac{\mathrm{d}z}{z^2} x C_{Lq}^{(1)}\left(\frac{x}{z}\right) N(z,Q^2) \tag{3.35}$$
$$+ \langle e^2\rangle \frac{\alpha_s}{2\pi}\int_x^1 \frac{\mathrm{d}z}{z^2} x C_{Lq}^{(1)}\left(\frac{x}{z}\right) \Omega(z,Q^2)$$
$$+ \langle e^2\rangle \frac{\alpha_s}{2\pi}\int_x^1 \frac{\mathrm{d}z}{z^2} x C_{Lg}^{(1)}\left(\frac{x}{z}\right) G(z,Q^2),$$

where

$$N(x,Q^2) = x\sum_{i=1}^{N_F} e_i^2 q_i^+(x,Q^2). \tag{3.36}$$

With this, the PDFs calculated in this thesis can be related to the structure functions, DIS cross sections and experimental data. The nonlinear gluon recombination corrections enter the structure functions implicitly through $\Omega(x,Q^2)$ and $G(x,Q^2)$.

4 Numerical Method

The approach used by the program QCDNUM16 [9] to solve the DGLAP equations is explained and extended to the GLR-MQ equations.

4.1 Basic Principle

To solve the evolution equations, they are evaluated numerically on an x-Q^2-grid. Given the parton distributions at a starting value Q_0^2, the distributions at other values of Q^2 are determined by solving a set of four equations at each grid point. In the following, these equations are derived using spline interpolation between grid points.

The grid consists of $n+1$ values of x bounded by x_0 and 1, i.e. $x_0 < \ldots < x_n = 1$, and $m+1$ values of Q^2 which are all above or below Q_0^2. Around 50 values are used for both x and Q^2 in this thesis, spaced logarithmically because the region of low x and Q^2 is most relevant here. In the following, $D(x_c, Q_r^2) = D_{rc}$ refers to $\Omega(x, Q^2)$ or $G(x, Q^2)$ evaluated at the grid point (x_c, Q_r^2), and the logarithmic derivative $\partial D / \partial \ln Q^2$ is written as D'. At $x = 1$, D is set to zero, so $D_{rn} = 0$ for all r.

In order to compute the integrals in eqs. (3.18), (3.19) and (3.29), D is interpolated linearly between x-values,

$$D_x(x, Q_r^2) = a_1 x + a_0 \text{ with } x \in [x_k, x_{k+1}]. \tag{4.1}$$

By imposing the continuity condition $D_x(x_i, Q_r^2) = D_{ri}$ for $i = k, k+1$, one obtains

$$D_x(x, Q_r^2) = (1 - t_k)\, D_{rk} + t_k\, D_{r(k+1)} \text{ with } t_k = \frac{x - x_k}{x_{k+1} - x_k} \in [0, 1]. \tag{4.2}$$

With this, the integrals can be written as weighted sums over D_{rk}, where k runs from c to n. Assuming D_{rk} is known for $k > c$ (condition 1), the only unknowns in the DGLAP equations are $\Omega_{rc}, \Omega'_{rc}, G_{rc}$ and G'_{rc}.

Two more equations relating these unknowns can be obtained by using a quadratic interpolation between Q^2-values,

$$D_Q(x_c, Q^2) = a_2 \left(\ln Q^2\right)^2 + a_1 \ln Q^2 + a_0 \text{ with } Q^2 \in \left[Q_{r-1}^2, Q_r^2\right]. \tag{4.3}$$

The requirements $D_Q(x_c, Q_i^2) = D_{ic}$ and $D'_Q(x_c, Q_i^2) = D'_{ic}$ for $i = r-1, r$ imply

$$D_{rc} = D_{(r-1)c} + \frac{\Delta_r}{2}\left(D'_{(r-1)c} + D'_{rc}\right), \tag{4.4}$$

with $\Delta_r = \ln Q_r^2 - \ln Q_{r-1}^2$. If $D_{(r-1)c}$ and $D'_{(r-1)c}$ have been calculated during the previous evolution steps (condition 2), eq. (4.4) and the DGLAP equations can be solved for the four unknowns.

The path through the grid must now be chosen such that conditions 1 and 2 are satisfied for any grid point (x_c, Q_r^2) where D is being evaluated. This is achieved by starting at $x_n = 1$ for every value of Q^2 and proceeding towards smaller x, as illustrated in fig. 7.

Throughout the numerical analysis, the coupling α_s is computed with eq. (2.5). The scale parameter Λ in that equation is calculated before the evolution by using the starting value $\alpha_s(M_Z^2) = 0.118$ (with the Z boson mass $M_Z = 91.2\,\text{GeV}$) and requiring $\alpha_s(Q^2)$ to be continuous at the flavor thresholds $m_c = 1.3\,\text{GeV}$ and $m_b = 4.5\,\text{GeV}$.

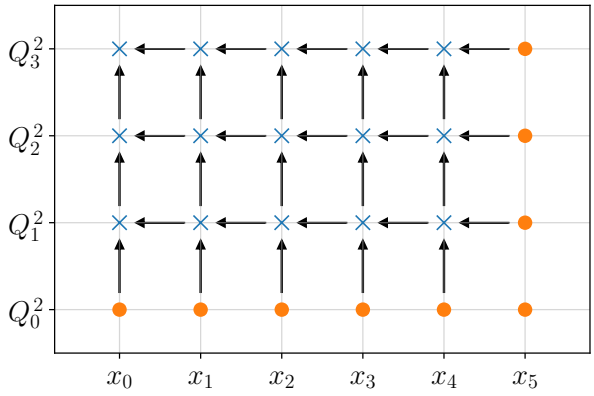

Fig. 7: The evolution path through a grid with $n = 5$ and $m = 3$. Every row is evaluated from the right to the left, starting at the bottom and going to the top. The orange dots indicate the starting values of D.

4.2 DGLAP

Using the linear interpolation in eq. (4.2), the convolution integrals in the DGLAP equations can be written as

$$\int_{x_c}^{1} \frac{\mathrm{d}z}{z^2} x_c P_{AB}\left(\frac{x_c}{z}\right) D(z, Q_r^2) = \sum_{k=c}^{n-1} w_{AB}(x_k, x_c)\, D_{rk}, \tag{4.5}$$

where

$$w_{AB}(x_k, x_c) = \begin{cases} S_1\left(f_{c+1}, f_c\right) \text{ if } k = c \\ S_1\left(f_{k+1}, f_k\right) - S_2\left(f_k, f_{k-1}\right) \text{ else} \end{cases} \tag{4.6}$$

with $f_k = x_c/x_k$ and

$$S_i(u, v) = \frac{a_i}{v-u} \int_u^v \frac{\mathrm{d}z}{z}(z - b_i) P_{AB}(z), \tag{4.7}$$
$$a_1 = b_2 = v,\ a_2 = b_1 = u.$$

The weights $w_{AB}(x_k, x_c)$ are calculated numerically at program initialisation.

The discretised DGLAP equations can then be expressed as

$$\Omega'_{rc} = W_{FF}\Omega_{rc} + W_{FG}G_{rc} + M_F \tag{4.8}$$
$$G'_{rc} = W_{GF}\Omega_{rc} + W_{GG}G_{rc} + M_G, \tag{4.9}$$

where $W_{AB} = (\alpha_s/2\pi)\, w_{AB}(x_c, x_c)$ and M_F, M_G contain the summands with $k > c$ multiplied by $(\alpha_s/2\pi)$. Together with eq. (4.4), they form a system of four linear equations with four unknowns. This system is solved numerically at every step in the evolution.

In order to test its accuracy, the evolution was done with nCTEQ15 PDFs [13] for different nuclei at $Q_0 = 2\,\mathrm{GeV}$, evolving up to $Q_m = 10\,\mathrm{GeV}$ ($n = 50$, $m = 40$). The evolution results for Au-197 at $Q = 4\,\mathrm{GeV}, 10\,\mathrm{GeV}$ obtained with python are in almost perfect agreement with the corresponding nCTEQ15 parametrisation at those values, see fig. 8. The average relative discrepancy for $Q = Q_m$ and $10^{-5} \leq x \leq 10^{-3}$ is around 1.2% for both the quark singlet and the gluon distribution.

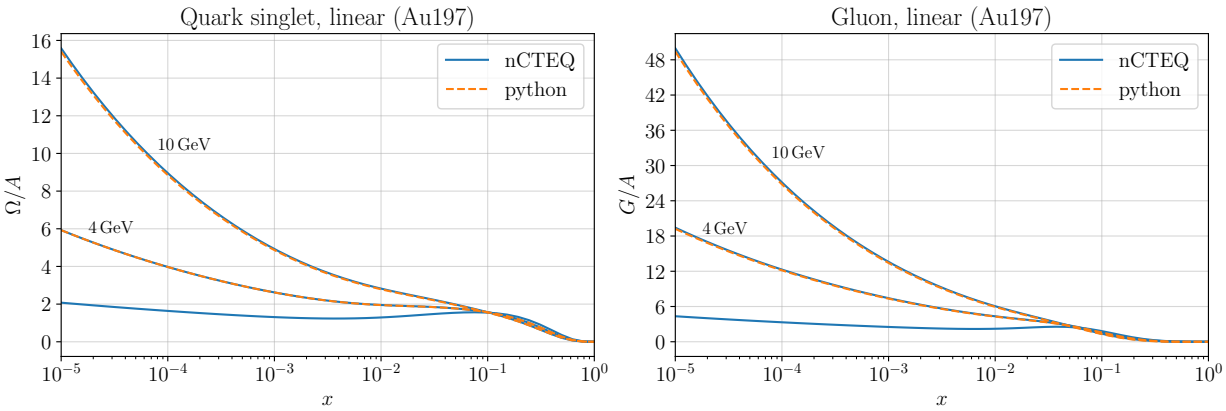

Fig. 8: Results of the (upward) DGLAP evolution using nCTEQ15 PDFs [13] at $Q_0 = 2\,\text{GeV}$ as input, compared with the PDFs at 4 GeV and 10 GeV.

4.3 GLR-MQ

Inserting eq. (4.2) into the GLR-MQ correction term in the gluon evolution in eq. (3.29) yields

$$\int_{x_c}^{1} \frac{\mathrm{d}z}{z}\, G^2(z, Q_r^2) = \sum_{k=c}^{n-1} w_1(x_k)\, G_{rk}^2 + \sum_{k=c}^{n-2} 2w_2(x_k)\, G_{r(k+1)} G_{rk}, \tag{4.10}$$

with

$$w_1(x_k) = \begin{cases} T_1(x_c, x_{c+1}) \text{ if } k = c \\ T_1(x_k, x_{k+1}) + T_2(x_{k-1}, x_k) \text{ else} \end{cases} \tag{4.11}$$

$$w_2(x_k) = -T_3(x_k, x_{k+1}) \tag{4.12}$$

and

$$T_i(u, v) = \frac{1}{(v-u)^2} \int_u^v \frac{\mathrm{d}z}{z} \big(c_i d_i - (c_i + d_i)z + z^2\big), \tag{4.13}$$

$$c_1 = d_1 = d_3 = v,\ c_2 = d_2 = c_3 = u.$$

The computation of $w_1(x_k)$ and $w_2(x_k)$ can be done much faster than that of the DGLAP weights $w_{AB}(x_k, x_c)$: Only $O(n)$ integrals must be calculated instead of $O(n^2)$, and the integrand in eq. (4.13) is a great deal simpler than the splitting functions in eq. (4.7).

With this and the results from the previous section, the GLR-MQ equations become

$$\Omega'_{rc} = W_{FF}\Omega_{rc} - V_1 G_{rc}^2 + W_{FG} G_{rc} + M_F \tag{4.14}$$

$$G'_{rc} = W_{GF}\Omega_{rc} - V_2 G_{rc}^2 + (W_{GG} - V_3) G_{rc} + M_G - N_G, \tag{4.15}$$

where $V_1 = (27/160) f(Q_r^2)$, $V_2 = (81/16) f(Q_r^2) w_1(x_c)$, $V_3 = (81/16) f(Q_r^2) 2w_2(x_c) G_{r(c+1)}$. The term N_G contains the remainder of the sums in eq. (4.10) multiplied by $(81/16) f(Q_r^2)$. Eq. (4.4) still applies, so again there are four equations relating D_{rc} and D'_{rc} that can be solved at each grid point when using the evolution path in fig. 7.

4.4 Python Code

All computation times listed in this section were recorded with `timeit` for a 50×40-grid on a PC using 600-800 MB of RAM.

The central part of the code written for this thesis is a python class which handles the whole evolution. At initialisation, the weights for the convolution integrals are calculated using the module `scipy.integrate`. This is the most computationally intensive step and takes comparatively long (around 3.3 min) since $O(n^2)$ integrals over the splitting functions in sec. 7.1 need to be evaluated, but it only has to be done once for a given grid. It can also be avoided completely by saving the weight tables after calculating them once.

After loading the input PDFs, the evolution proceeds as shown in fig. 7. The equations derived in the previous sections are solved with `scipy.optimize` at every grid point, and the results for any row (or column) of the grid can be extracted at the end. The evolution takes about 0.5 s for the DGLAP equations and 0.7 s for GLR-MQ.

Three booleans (`mix,nlo,nonlin`) are passed to the class to switch quark-gluon mixing, the NLO contributions to the splitting functions and the nonlinear terms on or off independently. This allows comparing the impact of different contributions to the GLR-MQ equations. Also, the weight calculation runs much faster at LO (around 5.6 s) or without mixing (around 1.4 min), which can be useful when qualitative results are sufficient.

Objects of the python class have the following attributes:

- `x,q` - 1D arrays containing $x_0, \ldots, x_n$ and $Q_0^2, \ldots, Q_m^2$ respectively
- `nx,nq` - equal to $n+1$ and $m+1$
- `mix,nlo` - booleans, as explained above
- `Qu,Gl` - 3D arrays containing D_{rc} and D'_{rc} for each grid point
- `wff,wfg,wgf,wgg` - 3D arrays containing the DGLAP integral weights for every combination (x_k, x_c) with $k \geq c$ and every value of Q_r^2
- `w1,w2` - 1D arrays containing the GLR-MQ integral weights for each x_c

The methods provided by the class are:

- `__init__(self,x,q,mixing,nlo)` - initialises the class object; `x` and `q` are 1D arrays containing the desired values of x and Q^2
- `weights(self)` - calculates the convolution weights
- `load_values(self,array_Qu,array_Gl,nonlin,A)` - loads the 1D arrays `array_Qu` and `array_Gl` as starting values and calculates D'_{0c} for all c; `A` is the mass number corresponding to the input PDFs
- `evolve(self,r,nonlin,A)` - runs the evolution step $Q_{r-1} \to Q_r$
- `evolve_all(self,nonlin,A)` - runs the complete evolution
- `res(self,r,D)` - returns a PDF at Q_r as a 1D array; `D` is a string determining if G (`D = 'Gluon'`) or Σ (`D = 'Quark singlet'`) is returned
- `__str__(self)` - prints the parameters of the class object

5 Results

The numerical solutions of the DGLAP and the GLR-MQ equations obtained with python are presented and discussed in this section.

5.1 Evolution Direction

The quadratic terms in the GLR-MQ equations are proportional to $1/Q^2$, so they can be neglected at high Q. This is supported by the fact that the difference between the GLR-MQ and the DGLAP PDFs is very small above $Q = 10\,\mathrm{GeV}$, see fig. 9. As a consequence, the evolution should give a more accurate picture of the quadratic terms' effect when evolving downward from high Q_0 (since the input doesn't take gluon recombination into account). Still, both evolution directions will be discussed here.

The results of the upward and downward nonlinear evolutions for Au-197 are shown in fig. 10. Au-197 was chosen since the gluon recombination effects are more pronounced for heavy nuclei, see section 5.3. Here and in the following, nCTEQ15 PDFs [13] are always used as starting values, on a grid with $n = 50$ and $m = 40$.

In the case of the upward evolution, both $\Omega(x, Q^2)$ and $G(x, Q^2)$ at $Q_m = 10\,\mathrm{GeV}$ are below the corresponding nCTEQ15 PDFs at low x. This shows that gluon recombination contributes to taming down the asymptotic growth of the PDFs in this region, as discussed in other papers [21, 22, 23].

Physically, the decrease in $G(x, Q^2)$ can be explained with the recombination of low-x gluons into high-x gluons. The g-q splitting function $P_{FG}(x/z)$ is positive for $x \leq z \leq 1$, so the lower gluon PDFs lead to a smaller rate of change $\Omega'(x, Q^2)$ and consequently to the observed decrease in $\Omega(x, Q^2)$. The absolute difference between GLR-MQ and DGLAP PDFs is generally smaller for the quark distribution though.

For the downward evolution, $\Omega(x, Q^2)$ at $Q_m = 2\,\mathrm{GeV}$ and low x is decreased compared to the nCTEQ15 PDFs, while $G(x, Q^2)$ is increased. The relative discrepancy between python and nCTEQ15 results is also notably bigger than with the upward evolution, especially at low x. This is because the DGLAP PDFs are much smaller at $Q_m = 2\,\mathrm{GeV}$; the absolute difference between GLR-MQ and DGLAP PDFs at $x = 10^{-5}$ and $Q = Q_m$ is similar for both directions.

The gluon distribution at the end of the downward evolution can be seen as a consequence of reversed g-g recombination, i.e. the migration of high-x gluons towards low x. As before, the change in $G(x, Q^2)$ affects $\Omega(x, Q^2)$, mostly through $P_{FG}(x/z)$. The reversed g-q splitting behaves like quark-antiquark pairs recombining into gluons, which explains the decrease in $\Omega(x, Q^2)$.

5.2 Parton Mixing

Mixing (q-g and g-q splitting) is the mechanism that drives the interaction between $G(x, Q^2)$ and $\Omega(x, Q^2)$ in the DGLAP equations. The GLR-MQ equations can be solved without mixing, i.e. for $P_{FG} \equiv P_{GF} \equiv 0$ (`mix=False` in python), to isolate the gluon recombination effects.

The results are shown in fig. 11. The quark distribution barely changes during the evolution, so the combined effect of the q-q splitting and the g-q recombination is very small compared to that of the neglected g-q splitting. Consequently, the differences between the

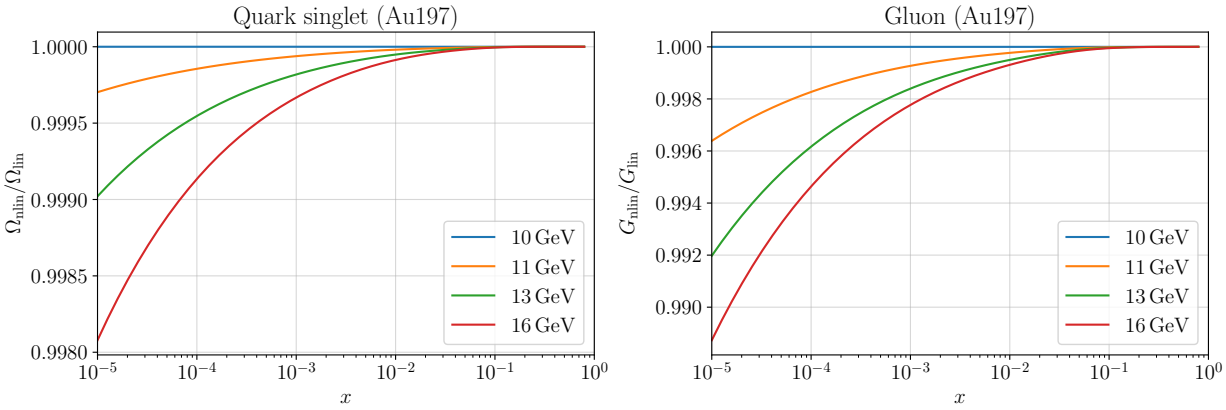

Fig. 9: Ratio of the GLR-MQ (nlin) and DGLAP (lin) PDFs after the evolution from $Q_0 = 10\,\mathrm{GeV}$ to $Q_m = 16\,\mathrm{GeV}$ with input from nCTEQ15 [13].

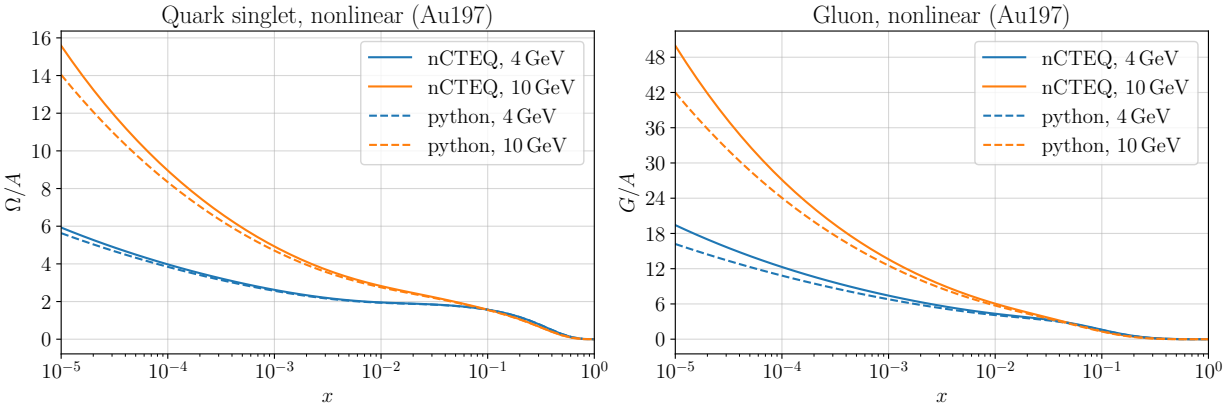

(a) $Q_0 = 2\,\mathrm{GeV}$ (b) $Q_0 = 2\,\mathrm{GeV}$

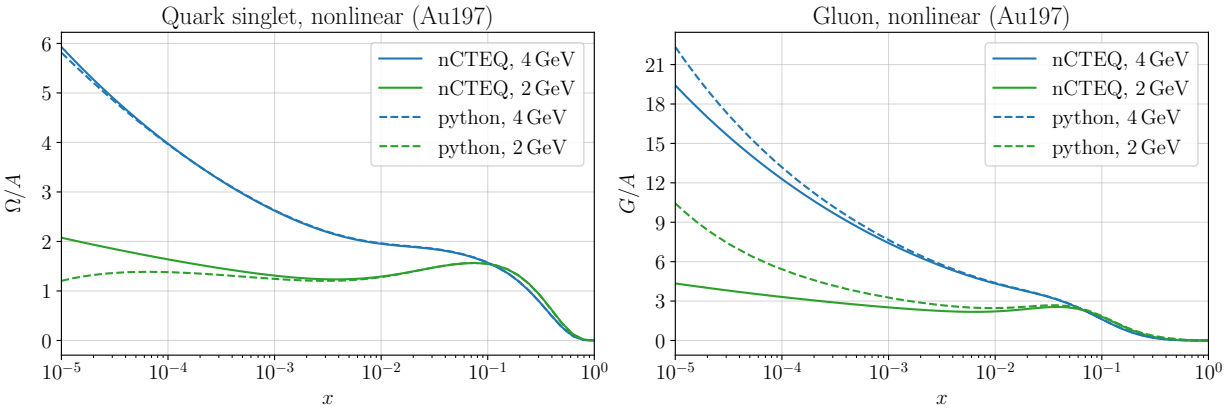

(c) $Q_0 = 10\,\mathrm{GeV}$ (d) $Q_0 = 10\,\mathrm{GeV}$

Fig. 10: Results of the GLR-MQ evolution for Au-197: (a,b) upward, (c,d) downward evolution.

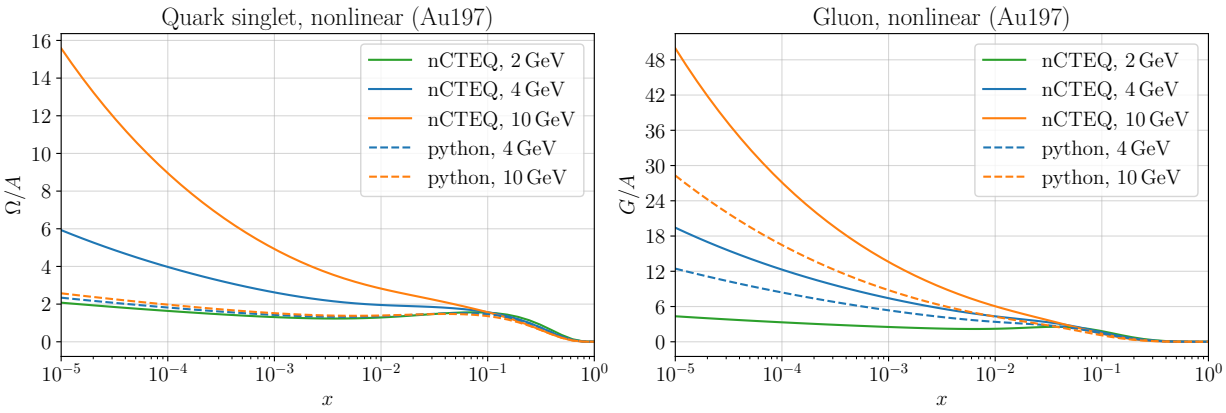

(a) $Q_0 = 2\,\mathrm{GeV}$

(b) $Q_0 = 2\,\mathrm{GeV}$

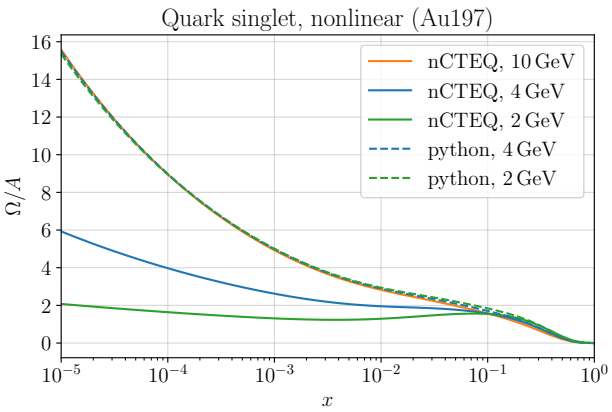

(c) $Q_0 = 10\,\mathrm{GeV}$

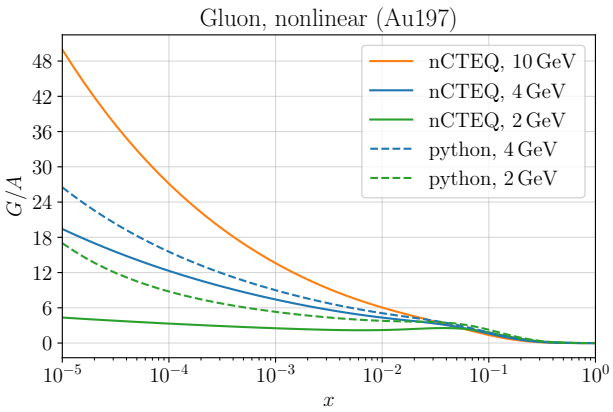

(d) $Q_0 = 10\,\mathrm{GeV}$

Fig. 11: Results of the evolution with $P_{FG} \equiv P_{GF} \equiv 0$.

GLR-MQ and the DGLAP PDFs can mainly be attributed to the quadratic term in eq. (3.29). This is consistent with the predictions made by Mueller and Qiu [8].

The gluon distribution also differs from the full result in fig. 10 significantly, especially in the low-x region. This is because the absence of q-g splitting leads to a decrease of $G'(x, Q^2)$, and thus to an increase or decrease of $G(x, Q^2)$ (depending on the evolution direction). Still, the combined g-g splitting and g-g recombination causes $G(x, Q^2)$ to change noticeably during the evolution, showing these effects aren't negligible compared to the q-g splitting.

5.3 A Dependence

When using the approximation $R \propto A^{1/3}$, the nonlinear terms in the GLR-MQ equations fall as $A^{-2/3}$. On the other hand, the nCTEQ15 gluon PDFs grow considerably with A, which counteracts the $A^{-2/3}$ behavior. In particular, assuming the nuclear PDFs scale as A (neglecting nuclear modifications of PDFs), the GLR-MQ terms scale as $A^{4/3}$.

The GLR-MQ/DGLAP ratios for the free proton as well as the nuclei C-12, Ca-40, Hs-108 and Au-197 are shown in fig. 12. As expected, they clearly differ more from one with increasing A. The upward evolution result for the proton gluon distribution is modified by about 4.5% at $x = 10^{-5}$, and the Au-197 distribution by about 15%.

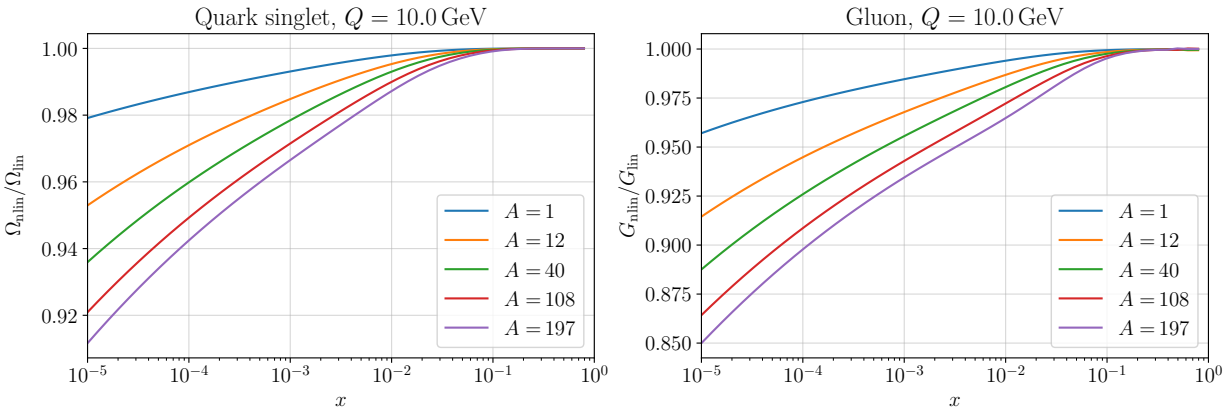

(a) $Q_0 = 2\,\mathrm{GeV}$

(b) $Q_0 = 2\,\mathrm{GeV}$

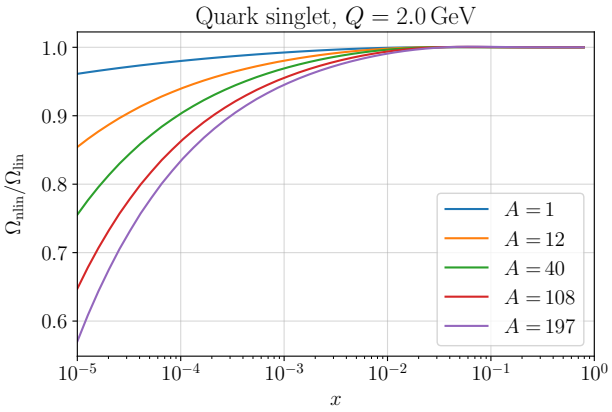

(c) $Q_0 = 10\,\mathrm{GeV}$

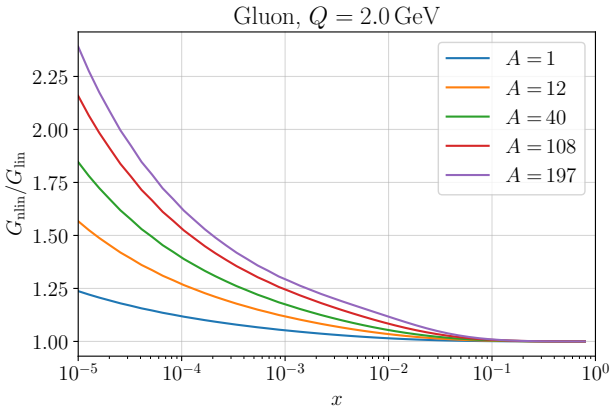

(d) $Q_0 = 10\,\mathrm{GeV}$

Fig. 12: Ratio of the GLR-MQ/DGLAP evolution results for different nuclei.

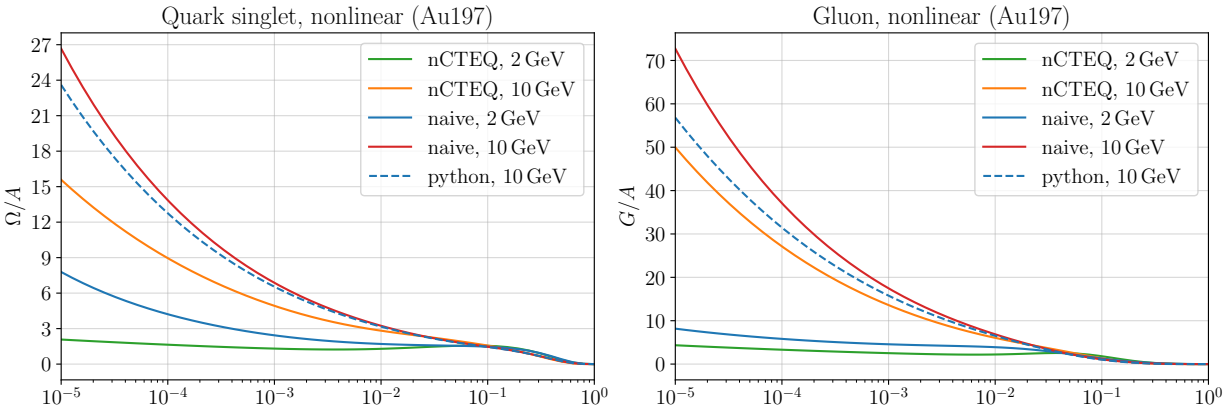

Fig. 13: Results of the nonlinear upward evolution with naive superpositions as input ($Q_0 = 2\,\mathrm{GeV}$).

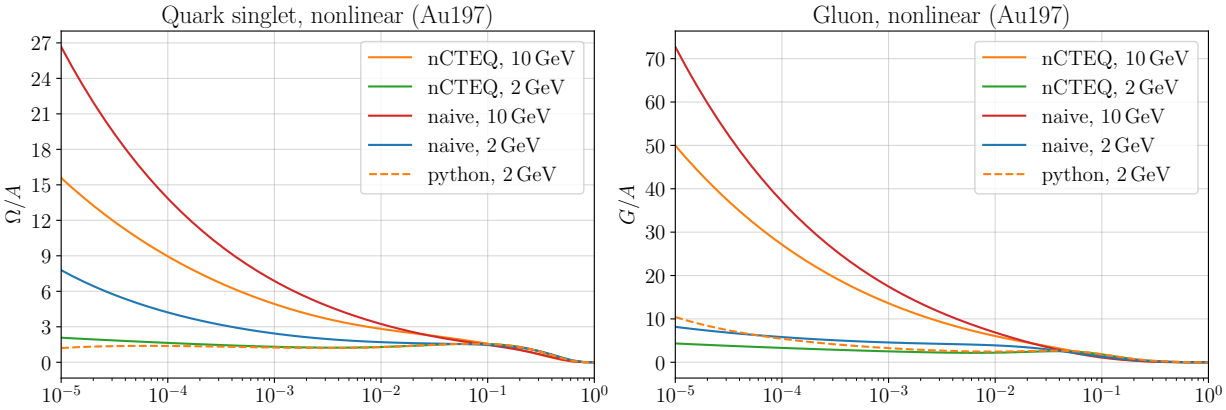

Fig. 14: Results of the nonlinear downward evolution with nCTEQ15 PDFs as input ($Q_0 = 10\,\text{GeV}$).

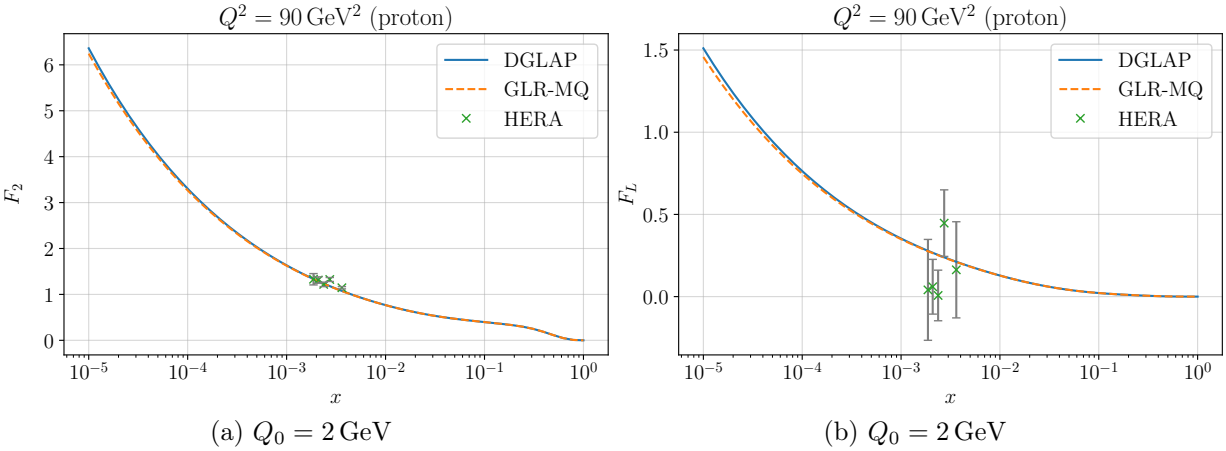

(a) $Q_0 = 2\,\text{GeV}$ (b) $Q_0 = 2\,\text{GeV}$

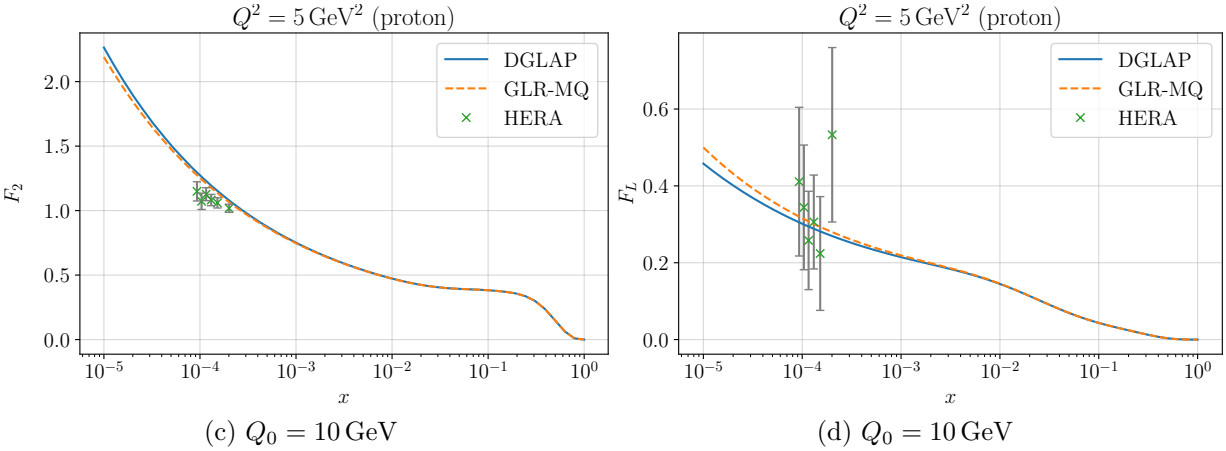

(c) $Q_0 = 10\,\text{GeV}$ (d) $Q_0 = 10\,\text{GeV}$

Fig. 15: Structure functions F_2 and F_L compared to data from HERA [24].

For $x \geq 10^{-1}$, the difference between the GLR-MQ and DGLAP PDFs is close to zero, and it grows steadily toward low x. This behavior matches the approximate analytical solutions of other groups [21, 22, 23]. It is also apparent that the nonlinear terms have a much bigger relative impact on the downward evolution, as explained in sec. 5.1.

The initial values from the nCTEQ15 parametrisation are based on experimental data, and hence affected by small-x nuclear effects like shadowing [13]. To investigate how these effects compete with gluon recombination, a "naive" superposition of free proton and neutron PDFs was considered, i.e.

$$\Sigma_A(x, Q_0^2) = Z \cdot \Sigma_p(x, Q_0^2) + N \cdot \Sigma_n(x, Q_0^2) = A \cdot \Sigma_p(x, Q_0^2) \tag{5.1}$$

$$g_A(x, Q_0^2) = Z \cdot g_p(x, Q_0^2) + N \cdot g_n(x, Q_0^2) = A \cdot g_p(x, Q_0^2). \tag{5.2}$$

The proton/neutron PDFs are related through isospin symmetry [1], implying $\Sigma_n \equiv \Sigma_p$ and $g_n \equiv g_p$. At low x, the superpositions Σ_A and g_A are increased compared to the PDFs with nuclear modifications, which amplifies the impact of gluon recombination.

The "naive" PDFs were used as input for an upward evolution, see fig. 13. The low-x results at $Q_m = 10\,\mathrm{GeV}$ are closer to the actual nCTEQ15 PDFs than $\Omega_A \equiv x\Sigma_A$ and $G_A \equiv xg_A$ at that value, especially for $G(x, Q^2)$. This suggests other nuclear effects have a bigger impact on the quark distribution. Still gluon recombination appears to be a significant contribution to the suppression of nuclear PDFs observed in experiments.

This can be probed further by using a nonlinear downward evolution with nCTEQ15 PDFs as input (which corresponds to reversing gluon recombination effects), and comparing the results to $\Omega_A(x, Q^2)$ and $G_A(x, Q^2)$. This is shown in fig. 14. As one would expect, the evolved gluon distribution at low x is closer to $G_A(x, Q^2)$ than to the actual nCTEQ15 PDF. The same isn't true for the quark distribution, again supporting the idea that other effects are more important here.

5.4 Structure Functions

The GLR-MQ PDFs can be related to experimental data by computing the corresponding structure functions F_2 and F_L with eqs. (3.34) and (3.35). The convolution integrals in these equations have exactly the same structure as those in the DGLAP equations, so the method explained in sec. 4.2 can be used to evaluate them. The non-singlet PDFs $N(x, Q^2)$ are taken directly from nCTEQ15 since their evolution is independent of $G(x, Q^2)$.

Using $N(x, Q^2)$ and the quark singlet and gluon PDFs calculated with python, the structure functions in fig. 15 were obtained. Experimental data from the particle accelerator HERA [24] for the proton is also shown. The difference between the DGLAP and the GLR-MQ structure functions is quite small, which makes sense considering the same is true for the proton PDFs (see fig. 12). Still it appears the nonlinear corrections improve the agreement between theory and data, if only slightly.

The ratio of the GLR-MQ/DGLAP structure functions for different nuclei is shown in fig. 16. It mirrors the A dependence of the PDFs in fig. 12, where F_2 is apparently dominated by $\Omega(x, Q^2)$ and F_L by $G(x, Q^2)$. The nonlinear effects are again most important for heavy nuclei, and their impact is larger for F_L than for F_2, so it should be easier to observe them experimentally when measuring F_L. For instance, when evolving upward the structure function F_L for the proton is modified by about 3.5% at $x = 10^{-5}$, see fig. 16b. A similar-size discrepancy can already be observed at $x = 4 \cdot 10^{-3}$ for Au- 197.

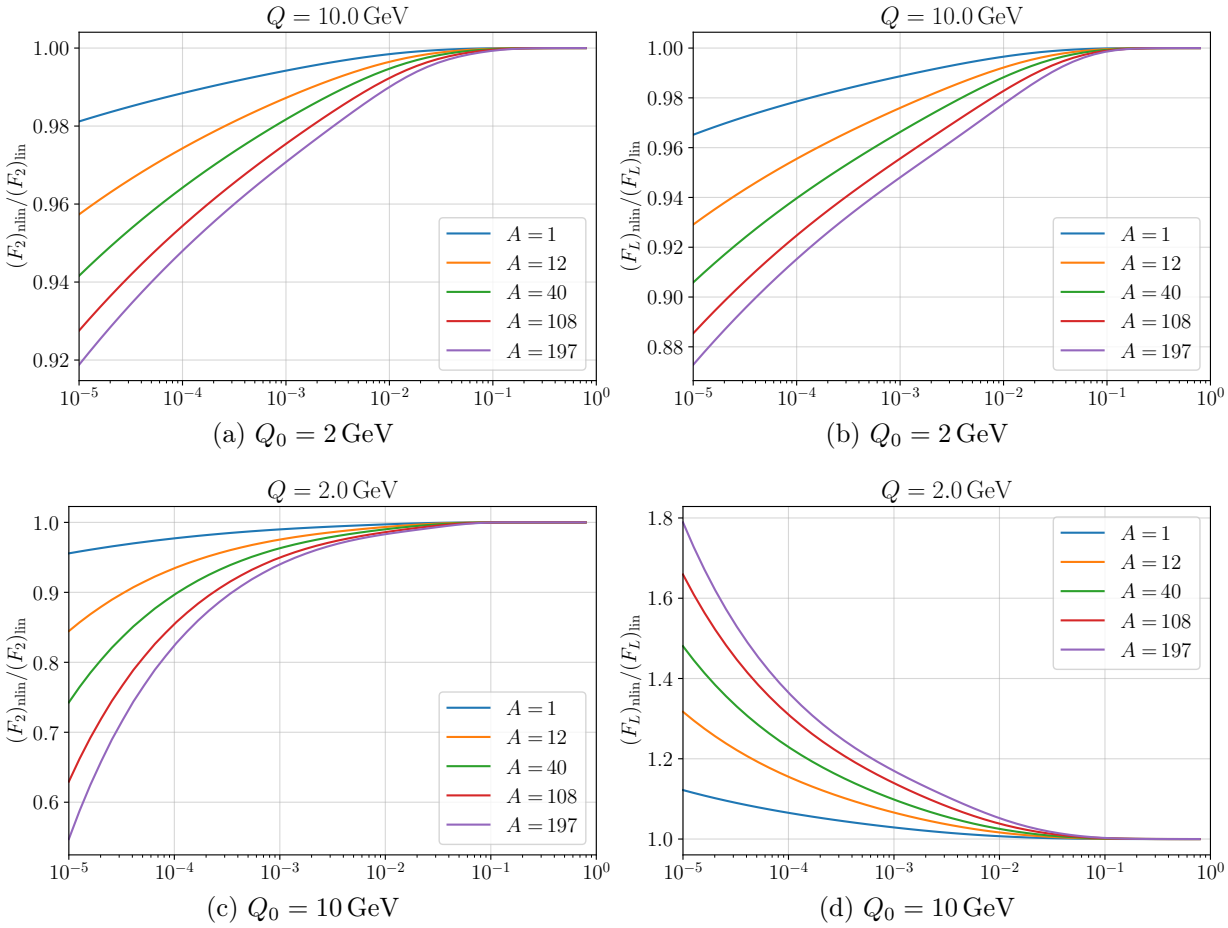

(a) $Q_0 = 2\,\mathrm{GeV}$ (b) $Q_0 = 2\,\mathrm{GeV}$

(c) $Q_0 = 10\,\mathrm{GeV}$ (d) $Q_0 = 10\,\mathrm{GeV}$

Fig. 16: Ratio of the GLR-MQ/DGLAP structure functions for different nuclei.

It will be possible to obtain lepton-nucleus DIS data for $x \sim 10^{-4}$ at low perturbative values of Q^2 (around $1\,\mathrm{GeV}^2$) at the EIC [25], and even for $x \sim 10^{-6}$ at the LHeC [26]. Together with fig. 16, this implies gluon recombination effects should be detectable at those facilities.

6 Summary

The cross section for lepton-nucleus DIS can be expressed in terms of universal PDFs using the QCD factorisation theorem. Due to parton emission processes the PDFs depend on the momentum transfer Q^2, an effect described by the DGLAP evolution equations. Gluon recombination effects lead to corrections to those equations, culminating in the nonlinear GLR-MQ equations. Both DGLAP and GLR-MQ equations were solved numerically with python for this thesis, and the influence of various parameters on the results was investigated.

The numerical evolution was done both with increasing and decreasing Q^2, and the physical implications were discussed. Among other things, it was concluded that the impact of the recombination terms on the results becomes larger towards low x, is negligibly small above $Q = 10\,\mathrm{GeV}$, and is greater when evolving downwards (relative to the regular DGLAP PDFs).

It was also investigated how the absence of parton mixing affects the evolution. The results show that the importance of g-q recombination is very small compared to g-q splitting and g-g recombination.

The ratio GLR-MQ/DGLAP was compared for different nuclei, with A ranging between 1 (proton) and 197 (Au-197). The recombination effects are more prominent for heavy nuclei. For example, the nonlinear corrections decrease $G(x = 10^{-5}, Q^2 = 100\,\mathrm{GeV}^2)$ by 4.5% for $A = 1$ and by 15% for $A = 197$ (when starting the evolution at $Q_0 = 2\,\mathrm{GeV}$). The relative difference is generally much bigger when evolving downward from $Q_0 = 10\,\mathrm{GeV}$. The interplay between gluon recombination and other nuclear effects (e.g. shadowing) was also discussed briefly.

Finally, the structure functions F_2 and F_L were calculated with the PDFs from the GLR-MQ evolution. Experimental data from HERA indicates that the nonlinear corrections slightly increase the accuracy of the theoretical prediction. It was also shown that gluon recombination effects in heavy nuclei should be observable at the EIC and the LHeC, especially when measuring F_L: Using GLR-MQ instead of DGLAP PDFs leads to a 12% decrease in $F_L(x = 10^{-5}, Q^2 = 100\,\mathrm{GeV}^2)$ for $A = 197$ (again using $Q_0 = 2\,\mathrm{GeV}$).

The results of this thesis could be used to include the GLR-MQ corrections in global PDF analyses like nCTEQ15. This should improve the resulting fits, especially for heavy nuclei in the low-Q^2 regime.

Further research could look into how the NNLO corrections to the splitting functions P_{AB} and the coupling parameter α_s alter the numerical GLR-MQ evolution. Also, the higher-twist contribution to g-q recombination given by Mueller and Qiu could be implemented to observe how it affects the results. Potential gluon recombination corrections to F_2, F_L could be adressed as well.

7 Appendix

7.1 Splitting Functions

The splitting functions P_{AB} can be written as a perturbation series in α_s, here up to NLO:

$$P_{AB}(x) = P_{AB}^{(0)}(x) + \frac{\alpha_s}{2\pi} P_{AB}^{(1)}(x). \tag{7.1}$$

The LO contributions are given by [9, 27]

$$P_{FF}^{(0)}(z) = C_F \big[p_{FF}(z)\big]_+ \qquad P_{FG}^{(0)}(z) = C_F\, p_{FG}(z) \tag{7.2}$$

$$P_{GF}^{(0)}(z) = 2T_R N_F\, p_{GF}(z) \quad P_{GG}^{(0)}(z) = 2C_G \frac{1}{z}\big[z\, p_{GG}(z)\big]_+ - \delta(1-x)\frac{2}{3} T_R N_F \tag{7.3}$$

where

$$p_{FF}(z) = \frac{1+z^2}{1-z} \qquad p_{FG}(z) = \frac{2}{z} - 2 + z \tag{7.4}$$

$$p_{GF}(z) = z^2 + (1-z)^2 \quad p_{GG}(z) = \frac{1}{1-z} + \frac{1}{z} - 2 + z - z^2. \tag{7.5}$$

(Note: Ref. [27] uses a different index convention where P_{FG} and P_{GF} are swapped.) The group factors are given by $C_G = N = 3$, $C_F = 4/3$ and $T_R = 1/2$, and the so-called plus prescription is defined as

$$\big[f(x)\big]_+ = f(x) - \delta(1-x) \int_0^1 \mathrm{d}y\, f(y). \tag{7.6}$$

The NLO terms for spacelike processes (i.e. for $Q^2 > 0$, as is the case in DIS) are [27]

$$P_{AA}^{(1,s)}(z) = \frac{1}{z}\big[z\hat{P}_{AA}^{(1,s)}(z)\big]_+ - \delta(1-z) \int_0^1 \mathrm{d}y\, y\hat{P}_{AB}^{(1,s)}(y) \tag{7.7}$$

$$P_{AB}^{(1,s)}(z) = \hat{P}_{AB}^{(1,s)}(z) \text{ for } A \neq B, \tag{7.8}$$

with

$$\begin{aligned}
\hat{P}_{FF}^{(1,s)} = {} & C_F^2 \left[-1 + x + \left(\frac{1}{2} - \frac{3}{2}x\right)\ln x - \frac{1}{2}(1+x)\ln^2 x \right. \\
& \left. - \left(\frac{3}{2}\ln x + 2\ln x \ln(1-x)\right) p_{FF}(x) + 2p_{FF}(-x)\mathcal{S}(x)\right] \\
& + C_F C_G \left[\frac{14}{3}(1-x) + \left(\frac{67}{18} - \frac{\pi^2}{6} + \frac{11}{6}\ln x + \frac{1}{2}\ln^2 x\right) p_{FF}(x) - p_{FF}(-x)\mathcal{S}(x)\right] \\
& + C_F T_R N_F \left[-\frac{16}{3} + \frac{40}{3}x + \left(2 + 10x + \frac{16}{3}x^2\right)\ln x - \frac{112}{9}x^2 \right. \\
& \left. + \frac{40}{9}\cdot\frac{1}{x} - 2(1+x)\ln^2 x - \left(\frac{10}{9} + \frac{2}{3}\ln x\right) p_{FF}(x)\right]
\end{aligned} \tag{7.9}$$

$$\begin{aligned}\hat{P}_{FG}^{(1,s)} &= C_F^2\left[-\frac{5}{3}-\frac{7}{2}x+\left(2+\frac{7}{2}x\right)\ln x+\left(-1+\frac{1}{2}x\right)\ln^2 x-2x\ln(1-x)\right. \\ &\left.+\left(-3\ln(1-x)-\ln^2(1-x)\right)p_{FG}(x)\right] \\ &+C_FC_G\left[\frac{28}{9}+\frac{65}{18}x+\frac{44}{9}x^2-\left(12+5x+\frac{8}{3}x^2\right)\ln x+(4+x)\ln^2 x+2x\ln(1-x)\right. \\ &\left.+\left(\frac{1}{2}-\frac{\pi^2}{6}-2\ln x\ln(1-x)+\frac{1}{2}\ln^2 x+\frac{11}{3}\ln(1-x)+\ln^2(1-x)\right)p_{FG}(x)+p_{FG}(-x)\mathcal{S}(x)\right] \\ &+C_FT_RN_F\left[-\frac{4}{3}x-\left(\frac{20}{9}+\frac{4}{3}\ln(1-x)\right)p_{FG}(x)\right]\end{aligned} \tag{7.10}$$

$$\begin{aligned}\hat{P}_{GF}^{(1,s)} &= C_FT_RN_F\left[4-9x+(-1+4x)\ln x+(-1+2x)\ln^2 x+4\ln(1-x)\right. \\ &\left.+\left(10-\frac{2}{3}\pi^2+4\ln x-4\ln x\ln(1-x)+2\ln^2 x-4\ln(1-x)+2\ln^2(1-x)\right)p_{GF}(x)\right] \\ &+C_GT_RN_F\left[\frac{182}{9}+\frac{14}{9}x+\frac{40}{9}\cdot\frac{1}{x}+\left(\frac{136}{3}x-\frac{38}{3}\right)\ln x-4\ln(1-x)-(2+8x)\ln^2 x\right. \\ &\left.+\left(\frac{\pi^2}{3}-\frac{218}{9}+\frac{44}{3}\ln x+4\ln(1-x)-\ln^2 x-2\ln^2(1-x)\right)p_{GF}(x)+2p_{GF}(-x)\mathcal{S}(x)\right]\end{aligned} \tag{7.11}$$

$$\begin{aligned}\hat{P}_{GG}^{(1,s)} &= C_FT_RN_F\left[-16+8x+\frac{20}{3}x^2+\frac{4}{3}\cdot\frac{1}{x}-(6+10x)\ln x-2(1+x)\ln^2 x\right] \\ &+C_GT_RN_F\left[2-2x+\frac{26}{9}\left(x^2-\frac{1}{x}\right)-\frac{4}{3}(1+x)\ln x-\frac{20}{9}p_{GG}(x)\right] \\ &+C_G^2\left[\frac{27}{2}(1-x)+\frac{67}{9}\left(x^2-\frac{1}{x}\right)+\left(-\frac{25}{3}+\frac{11}{3}x-\frac{44}{3}x^2\right)\ln x+4(1+x)\ln^2 x\right. \\ &\left.+\left(\frac{67}{9}-\frac{\pi^2}{3}-4\ln x\ln(1-x)+\ln^2 x\right)p_{GG}(x)+2p_{GG}(-x)\mathcal{S}(x)\right],\end{aligned} \tag{7.12}$$

where

$$\begin{aligned}\mathcal{S}(x) &= \int_{z/(1+z)}^{1/(1+z)}\frac{\mathrm{d}x}{x}\ln\left(\frac{1-x}{x}\right) \\ &= -2\,\mathrm{Li}_2(-x)-2\ln x\ln(1+x)+\frac{1}{2}\ln^2 x-\frac{\pi^2}{6}.\end{aligned} \tag{7.13}$$

7.2 Coefficient Functions

The coefficient functions for calculating the structure functions F_2 and F_L are [9, 16]

$$C_{2q}^{(1)}(x) = C_F\left[\frac{1+x^2}{1-x}\left(\ln\frac{1-x}{x}-\frac{3}{4}\right)+\frac{1}{4}(9+5x)\right]_+ \tag{7.14}$$

$$C_{2g}^{(1)}(x) = 2N_FT_R\left[\left(x^2+(1-x)^2\right)\ln\frac{1-x}{x}+8x(1-x)-1\right] \tag{7.15}$$

$$C_{Lq}^{(1)}(x) = 2C_Fx \tag{7.16}$$

$$C_{Lg}^{(1)}(x) = 8N_FT_Rx(1-x). \tag{7.17}$$

The plus-prescription used in $C_{2q}^{(1)}$ was defined in the previous section.

7.3 Deutsche Zusammenfassung

Nach unserem aktuellen Erkenntnisstand besteht der Atomkern aus Protonen und Neutronen, die wiederum Quarks und Gluonen (kollektiv Partonen genannt) enthalten. Partonen sowie die starke Wechselwirkung zwischen ihnen können mit einer renormierbaren, nichtabelschen Eichtheorie namens Quantenchromodynamik (QCD) beschrieben werden.

Der sauberste Weg den Atomkern experimentell zu untersuchen ist die tief-inelastische Lepton-Nukleus-Streuung, bei der hochenergetische Leptonen von Hadronen gestreut werden, was zur Dissoziation des Targets führt. Der zugehörige Wirkungsquerschnitt kann mit dem QCD-Faktorisierungstheorem über universelle Partondichtefunktionen (PDFs) ausgedrückt werden, die (in erster Ordnung Störungstheorie) als Impulsverteilungen der Partonen verstanden werden können.

Aufgrund von partonischen Emissionsprozessen hängen die PDFs vom Impulsübertrag Q^2 der Kollision ab. Die Entwicklung der PDFs mit Q^2 wird von den DGLAP-Gleichungen beschrieben, die sich aus „Leiter" -Emissionsdiagrammen ergeben. Die Rekombination von Gluonen führt zu Korrekturen dieser Gleichungen, die in Form der nichtlinearen GLR-MQ-Gleichungen zusammengefasst werden können.

Sowohl die DGLAP- als auch die GLR-MQ-Gleichungen wurden im Rahmen dieser Arbeit mit python 3.8 numerisch gelöst. Der Fokus lag dabei auf dem Einfluss unterschiedlicher Parameter (die Richtung der Entwicklung, das Mischen von Quarks und Gluonen sowie die Massenzahl A) auf die Ergebnisse.

Zudem wurden mit den erhaltenen PDFs die Strukturfunktionen F_2 und F_L berechnet und mit HERA-Daten verglichen, und es wurden Vorhersagen zu Streuprozessen mit schweren Nuklei an den zukünftigen Einrichtungen EIC und LHeC getroffen.

8 References

[1] Francis Halzen, Alan D. Martin, and Nilotpal Mitra. *Quarks and Leptons: An Introductory Course in Modern Particle Physics*. John Wiley & Sons, 1984. ISBN: 9780471811879.

[2] Owe Philipsen. *QFT und das Standardmodell der Teilchenphysik*. Springer, 2018. ISBN: 9783662578193.

[3] George Sterman et al. "Handbook of perturbative QCD". In: *Reviews of Modern Physics* 67.1 (1995), p. 157. DOI: 10.1103/RevModPhys.67.157.

[4] Yuri L Dokshitzer. "Calculation of the structure functions for deep inelastic scattering and e+ e- annihilation by perturbation theory in quantum chromodynamics". In: *Zh. Eksp. Teor. Fiz* 73 (1977), p. 1216.

[5] V.N. Gribov and L.N. Lipatov. "Deep inelastic electron scattering in perturbation theory". In: *Physics Letters B* 37.1 (1971), pp. 78–80. DOI: 10.1016/0370-2693(71)90576-4.

[6] Guido Altarelli and Giorgio Parisi. "Asymptotic freedom in parton language". In: *Nuclear Physics B* 126.2 (1977), pp. 298–318. DOI: 10.1016/0550-3213(77)90384-4.

[7] Leonid Vladimirovič Gribov, Eugene M Levin, and Michail G Ryskin. "Semihard processes in QCD". In: *Physics Reports* 100.1-2 (1983), pp. 1–150. DOI: 10.1016/0370-1573(83)90022-4.

[8] Alfred H Mueller and Jianwei Qiu. "Gluon recombination and shadowing at small values of x". In: *Nuclear Physics B* 268.2 (1986), pp. 427–452. DOI: 10.1016/0550-3213(86)90164-1.

[9] M Botje. *QCDNUM16: A fast QCD evolution program*. 1997. URL: https://www.nikhef.nl/~h24/qcdcode/qcdnum1612.pdf.

[10] Michael E Peskin and Daniel V Schroeder. *An introduction to quantum field theory*. CRC press, 1995. ISBN: 9780201503975.

[11] Hannu Paukkunen. "Global analysis of nuclear parton distribution functions at leading and next-to-leading order perturbative QCD". In: *arXiv: High Energy Physics - Phenomenology* (2009).

[12] Jean-Jacques Aubert et al. "The ratio of the nucleon structure functions F_2^N for iron and deuterium". In: *Phys. Lett. B* 123 (1983), 275–278. 10 p. DOI: 10.1016/0370-2693(83)90437-9.

[13] K Kovařík et al. "nCTEQ15: global analysis of nuclear parton distributions with uncertainties in the CTEQ framework". In: *Physical Review D* 93.8 (2016), p. 085037. DOI: 10.1103/PhysRevD.93.085037.

[14] J. Rożynek and G. Wilk. "How the nuclear Fermi motion plus a simple statistical model explains the EMC effect". In: *Nuclear Physics A* 721 (2003), pp. C388–C391. DOI: https://doi.org/10.1016/S0375-9474(03)01076-5.

[15] Yuri Dokshitzer. *Basics of perturbative QCD*. Atlantica Séguier Frontières, 1991. ISBN: 9782863321010.

[16] W Furmanski and Roberto Petronzio. "Lepton-hadron processes beyond leading order in quantum chromodynamics". In: *Zeitschrift für Physik C Particles and Fields* 11.4 (1982), pp. 293–314. DOI: 10.1007/BF01578280.

[17] Andy Buckley et al. "LHAPDF6: parton density access in the LHC precision era". In: *The European Physical Journal C* 75.3 (2015), pp. 1–20. DOI: 10.1140/epjc/s10052-015-3318-8.

[18] Jianwei Qiu. "Nuclear shadowing at small values of x". In: *Nuclear Physics B* 291 (1987), pp. 746–764. DOI: 10.1016/0550-3213(87)90494-9.

[19] Kjell Prytz. "Signals of gluon recombination in deep inelastic scattering". In: *The European Physical Journal C-Particles and Fields* 22.2 (2001), pp. 317–321. DOI: 10.1007/s100520100775.

[20] Yuri V Kovchegov and Eugene Levin. *Quantum chromodynamics at high energy*. Cambridge University Press, 2012. DOI: 10.1017/CBO9781139022187.

[21] GR Boroun and S Zarrin. "An approximate approach to the nonlinear DGLAP evolution equation". In: *The European Physical Journal Plus* 128.10 (2013), p. 1. DOI: 10.1140/epjp/i2013-13119-8.

[22] M Lalung, P Phukan, and JK Sarma. "On phenomenological study of the solution of nonlinear GLR-MQ evolution equation beyond leading order". In: *Nuclear Physics A* 984 (2019), pp. 29–43. DOI: 10.1016/j.nuclphysa.2019.01.006.

[23] Mayuri Devee. "Nonlinear Effects in Singlet Quark Distribution Predicted by GLR-MQ Evolution Equation". In: *XXIII DAE High Energy Physics Symposium*. Springer. 2021, pp. 641–647. DOI: 10.1007/978-981-33-4408-2_88.

[24] V. Andreev et al. "Measurement of inclusive *ep* cross sections at high Q^2 at $\sqrt{s} =$ 225 and 252 GeV and of the longitudinal proton structure function F_L at HERA". In: *Eur. Phys. J. C* 74.4 (2014), p. 2814. DOI: 10.1140/epjc/s10052-014-2814-6.

[25] J. Beebe-Wang et al. "Conceptual Design Report for the Electron-Ion Collider". In: *Brookhaven National Laboratory* (2021). DOI: 10.2172/1765663.

[26] P. Agostini et al. "The Large Hadron-Electron Collider at the HL-LHC". In: *J. Phys. G* 48 (2020). Submitted to J.Phys., 110501. 373 p. DOI: 10.1088/1361-6471/abf3ba.

[27] W Furmanski and Roberto Petronzio. "Singlet parton densities beyond leading order". In: *Phys. Lett. B* 97.CERN-TH-2933 (1980), pp. 437–442. DOI: 10.1016/0370-2693(80)90636-X.